Recent advances in nanoporous materials for renewable energy resources conversion into fuels

Fu, Jintao; Detsi, Eric; De Hosson, Jeff Th M.

Published in:
Surface & Coatings Technology

DOI:
10.1016/j.surfcoat.2018.05.001

Publication date:
2018

Surface & Coatings Technology 347 (2018) 320–336

Contents lists available at ScienceDirect

Surface & Coatings Technology

journal homepage: www.elsevier.com/locate/surfcoat

Recent advances in nanoporous materials for renewable energy resources conversion into fuels

Jintao Fu[a], Eric Detsi[a], Jeff Th.M. De Hosson[b,*]

[a] Department of Materials Science & Engineering, University of Pennsylvania, Philadelphia, PA 19104-6272, USA
[b] Department of Applied Physics, Zernike Institute for Advanced Materials, University of Groningen, Nijenborgh 4, 9747 AG Groningen, The Netherlands

ARTICLE INFO

Keywords:
Nanoporosity
Catalysts
Water oxidation
Methanol oxidation
Carbon dioxide
Carbon monoxide

ABSTRACT

The continuous growth in energy production from non-renewable resources in order to meet the ever-increasing energy demand has given rise to serious environmental issues and moving toward renewable energy resources is necessary. Heterogeneous catalysts play a key role in the conversion of renewable resources into fuels and chemicals. The performance of heterogeneous catalysts is directly linked to their surface area, since the number of catalytic sites as well as the activity of each catalytic site increase with increasing effective footprint area of a catalyst. Therefore, nanoporous heterogeneous catalysts are very attractive, owing to their high internal surface areas and high density of active sites generated by curved internal surfaces. The overall catalytic performance of nanoporous heterogeneous catalysts can reach orders of magnitude higher than that of planar catalysts counterparts. This paper reviews recent progress toward the applicability of three-dimensional bulk nanoporous metals and their composites in (electro-)catalytic conversion of renewable resources into fuels and value-added chemicals. The primary focus is given to metal-based materials fabricated through dealloying. Dealloyed nanoporous metals and their composites can be used either directly as high-performance (electro-)catalysts, or indirectly as three-dimensional bulk current collectors along with poorly conducting electro-catalyst materials. Limitations of these material systems such as cost, scalability, and long-term stability in-service are discussed.

1. Introduction

Macrofoams, a class porous material with pore size on the order of tens of microns are very attractive for a variety of industrial applications owing to their unique properties. For example, aluminum macrofoam boasts a high stiffness-to-density ratio, high capacity for energy absorption during compression, high temperature resistance, electrical and thermal conductivity, good machinability and cheap production costs. Thanks to these remarkable properties, macrofoams are attractive in the construction and automotive industries, for example [1–4].

While macrofoams are common materials with known applications in industry, there is a class of materials known as nanofoams or nanoporous metals, characterized by pore and strut sizes being at the nanoscale. For a more conventional definition, the International Union of Pure and Applied Chemistry has categorized nanoporous materials into three groups, depending on the characteristic pore size: microporous (pore size under 2 nm), mesoporous (pore size between 2 and 50 nm), and macroporous (pore size above 50 nm) materials. While maintaining some attractive characteristics of cellular materials as their macrofoam counterparts, nanofoams uniquely possess properties that are beyond the limit of macrofoams. For instance, nanofoams have seen scalable applicability in nanofiltration systems, drug delivery platforms, catalysis, sensing and actuation [5–12]. Nanoporous materials are also expected to significantly contribute to energy applications. To meet the increasing demand for renewable energy, cost-effective and scalable methods are needed for the conversion of renewable resources into fuels and value-added chemicals [13,14]. The kinetics of chemical reactions involved in fuel production can be enhanced by heterogeneous catalysts [15,16]. Furthermore, the performance of heterogeneous catalysts is directly linked to the number of catalytic sites per unit surface area: the higher the effective surface area of a catalyst, the better it performs [17]. Heterogeneous catalysts with high internal surface areas are therefore very attractive. Three-dimensional (3D) bulk nanoporous metals (NPM) represent an emerging class of materials characterized by their high specific surface area, remarkable intrinsic physical and chemical properties, and a unique combination of the mechanical robustness of “dense” materials with the intriguing properties of “nano” materials.

Thanks to these remarkable properties, 3D NPMs are very attractive in catalysis and electro-catalysis applications where they are used to

* Corresponding author.
E-mail address: j.t.m.de.hosson@rug.nl (J.T.M. De Hosson).

https://doi.org/10.1016/j.surfcoat.2018.05.001
Received 2 March 2018; Received in revised form 28 April 2018; Accepted 1 May 2018
Available online 03 May 2018
0257-8972/

enhance the kinetics of chemical and electrochemical reactions in two ways: (i) Either directly as (electro-)catalysts; (ii) or indirectly as electrically conducting 3D framework (NPMF) current collectors in combination with poorly conducting electro-catalyst materials, to enhance the overall charge transfer in the corresponding NPMF/electro-catalyst composites.

To date, 3D NPMs have found great advantage and applicability in the field of (electro-)catalysis for fuel production (e.g. H_2O oxidation and CO_2 reduction) and fuel consumption (e.g. methanol oxidation) [17–21]. Beside the high effective surface area of these materials, their improved performance also arises from their intrinsic chemical and physical properties such as electrical conductivity [21]. Finally, the broad range of NPMs makes it possible to design high-performance catalysts directly through the Sabatier principle, by properly selecting from volcano plots NPMs that will exhibit optimal surface interaction with the substance to convert. State-of-the-art (electro-)catalytic processes for fuel production and fuel consumption include water oxidation reaction (WOR), methanol oxidation reaction (MOR), and carbon dioxide reduction (CDR).

(i) The water oxidation reaction (also referred to as oxygen evolution reaction – OER) is very attractive for sustainable fuels production. This is because beside the high abundance of water for large scale energy applications, electrons generated during water oxidation can reduce protons and CO_2 into H_2 and carbonaceous fuels, respectively [22]. This non-spontaneous reaction is commonly driven by an external bias voltage, and electro-catalysts are required to lower the value of this voltage.
(ii) Direct methanol fuel cells (DMFCs) have the advantage of simple operation and high energy density, and thus applicable in automobile and portable electronics [23]. The methanol oxidation reaction is critical in DMFCs, and similarly to WORs, (electro-)catalysts are required to enhance to kinetics of MORs and lower the reaction overpotential.
(iii) The electrochemical reduction of CO_2 into other reusable carbon fuels such as CO and CH_4 is desirable from the view of sustainability and environment protection [24–29]. However, CO_2 is a fully oxidized and one of the most stable molecule among carbon-based substances [30,31]. Thus, cost effective, high selectivity and high efficiency (electro-)catalysts that can lower thermodynamic barrier for CDR are required [30,32].

In this contribution, we will discuss recent progress toward the applicability of 3D NPMs in the above 3 fields. The primary focus will be on NPMs produced by selective alloy leaching, a process known as dealloying. After presenting state-of-the-art dealloying routes to NPM (electro-)catalysts, we will discuss recent achievements in electro-catalytic oxidation of water using metallic foams and NPM composites. Next, we will present the performance of NPMs as methanol oxidation (electro-)catalysts. Finally, the potential of NPMs as CO_2 reduction electro-catalysts will be discussed.

2. Fabrication of nanoporous metal catalysts

The most popular method for the fabrication of nanoporous metal catalysts corresponds to the conventional “dealloying” route in aqueous media. During this nanofabrication process, a sacrificial element, usually the most (electro)chemically active element, is preferentially removed from a parent alloy using an acidic or alkaline aqueous corroding medium; sometimes an external electrical bias voltage can be used to drive the dealloying process if the reactions involved are not spontaneous [33–43]. In the former case where no external electrical field is required to assist the dissolution of the sacrificial component, the leaching process is referred to as free corrosion dealloying [33]. Fig. 1a shows the typical 3D bicontinuous morphology of nanoporous gold (NP-Au) prepared by free corrosion dealloying of Au/Ag alloy and used as catalyst for selective oxidation of methanol at low temperatures [19].

Fig. 1b depicts a similar 3D bicontinuous morphology in nanoporous silver (NP-Ag) prepared by free corrosion dealloying of a Ag/Al alloy and used as electro-catalyst for selective reduction of carbon dioxide to carbon monoxide [17]. The NP-Ag electro-catalyst from Fig. 1b was prepared from a non-equilibrium single-phase Ag/Al parent alloy following a procedure reported earlier by DeHosson et al. [34].

Besides dealloying in aqueous media, recently several new dealloying approaches have been explored: Sieradzki and Chen reported on electrolytic dealloying in Li-based nonaqueous solutions [44]; Detsi and co-workers suggested the use of Mg-based nonaqueous solutions for the selective electrolytic corrosion of Mg-rich alloys [45]; Kato and co-workers reported on free corrosion dealloying by metallic melt, a leaching process during which a molten hot metal is used as corroding medium to selectively extract the most reactive component of a parent alloy, taking advantage of the difference in enthalpy of mixing between the underlying alloy elements and the molten hot metal [46]; Chen and co-workers reported on vapor phase dealloying, during which the sacrificial phase is selectively removed by thermal evaporation [47]. Thanks to these various but complementary nanofabrication methods, a broad range of NPMs can be made for various applications including (electro-)catalysis.

3. Water oxidation

3.1. Motivation and background

The high abundance of water and the possibility to use electrons generated through water oxidation to reduce protons and CO_2 into H_2 and carbonaceous fuels, respectively [22], make the water oxidation reaction (WOR) very attractive for sustainable production of fuels and value-added chemicals. Protons reduction into H_2 is commonly referred to as hydrogen evolution reaction (HER) and when electrons used to reduce these protons are generated from the WOR, the combined HER and WOR process is referred to as water splitting. In this section we will focus on the WOR. This non-spontaneous reaction is commonly driven by an external electrical bias voltage, and like in any non-spontaneous electrochemical process, the applied electrical bias voltage is always higher than the thermodynamic potential of the reactions involved.

This difference between the theoretical and applied voltages is known as overpotential. The three primary origins of an overpotential area: (i) the internal resistance of the system; (ii) the charge transfer resistance at the solid catalyst/electrolyte interface; and (iii) the activation overpotential associated with an energy barrier to overcome before the reaction can take place. This energy barrier is significantly low in catalysts. Hence (electro-)catalysts are used to lower the overall value of the bias voltage involved in the WOR. The mechanism of electro-catalytic oxidation of water has been widely investigated [48], and high-performance water oxidation electro-catalysts have been identified [21,49–51], among which NiFe-based oxides, cobalt phosphate and cobalt borate systems have been developed [51,52].

A major fundamental challenge in the field, which will be the focus of this section, is associated with the poor electrical conductivity of water oxidation electro-catalysts (i.e. resistance overpotential). Indeed, water oxidation reaction favorably proceeds on non-metallic surfaces [53]; however non-metallic materials used as electro-catalysts suffer from very poor electrical conductivity when their characteristic structure size is not in the sub-100 nm range. This issue represents a bottleneck in the development of robust and scalable water oxidation electro-catalysts. For our porous materials systems, the fact that water oxidation takes place on non-metals also means that NPMs cannot be used directly as water oxidation (electro-)catalysts.

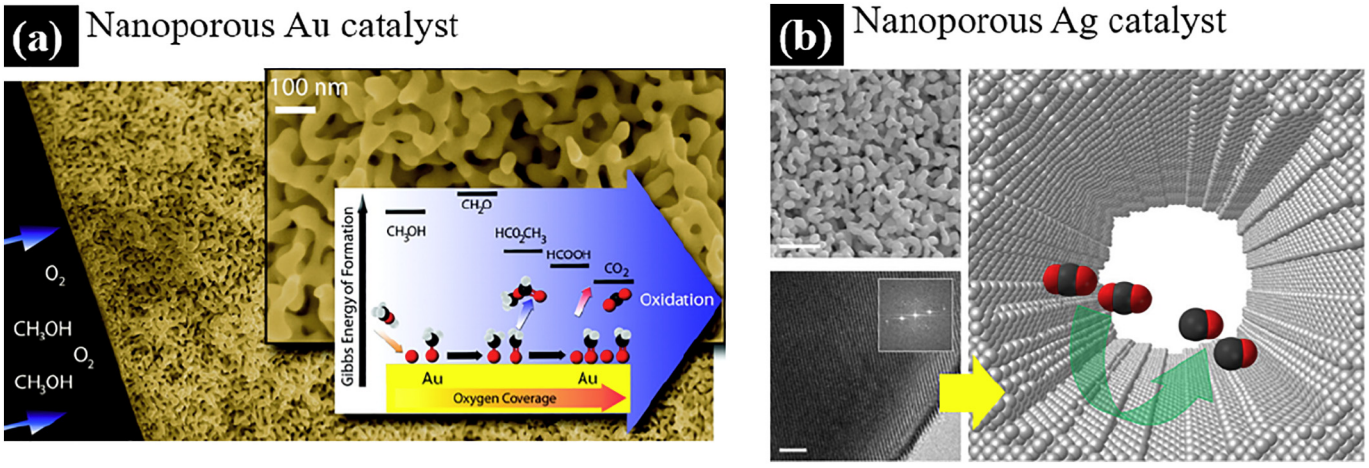

Fig. 1. (a) Typical 3D bicontinuous morphology of nanoporous gold catalyst at low and high magnifications, respectively. The nanoporous Au was prepared by dealloying of Au/Ag parent alloy (Reproduced from ref. [19]). (b) Similar 3D bicontinuous morphology in nanoporous silver catalyst prepared by dealloying of Ag/Al parent alloy following the procedure in ref. [34]. (For interpretation of the references to colour in this figure legend, the reader is referred to the web version of this article.) (For interpretation of the references to colour in this figure legend, the reader is referred to the web version of this article.)
(Reproduced from ref. [17])

3.2. Nanoporous metal/metal oxide composites

To find a way around this conductivity issue, some cellular materials have been proposed as 3D electrically conducting scaffolds (see Fig. 2a reproduced from [54]). In particular, state-of-the-art water oxidation electro-catalysts have been infiltrated into the pores of commercially available 3D nickel foams as illustrated in Fig. 2b and c reproduced from [52], to design robust electro-catalysts that can generate practical currents during water oxidation [52,55–58].

Thin films of Co-based water oxidation electro-catalysts can produce a current density of ~1 mA/cm^2 at ~410 mV overpotential near neutral pH [21,50]. As discussed earlier, this overpotential means that more energy is required than thermodynamically determined in order to drive a redox reaction. However, when these Co-based electro-catalysts are electrodeposited onto a 3D nickel foam scaffold to enhance their electrical conductivity, the corresponding water oxidation current density is increased from of ~1 mA/cm^2 to ~100 mA/cm^2 at 363 mV overpotential [21,52].

Another class of high-performance water oxidation electro-catalysts corresponds to NiFe oxides [21,49,59–62]. Thin films of NiFe-based water oxidation electro-catalysts can deliver a current density of ~10 mA/cm^2 at ~350 mV overpotential in 1 M alkaline solutions [21,49]. However, when NiFe-based water oxidation catalysts are grown onto 3D nickel foams to enhance their electrical conductivity, they only require 240 mV overpotential (instead of ~350 mV) to achieve a current density of ~10 mA/cm^2 in 1 M NaOH solution [21,55]; and they can deliver a current density of ~500 mA/cm^2 in 10 M KOH [21,56].

Despite this enhancement when Ni foams are used as 3D substrates and water oxidation electro-catalysts supported onto 3D nickel foams, there are advantages and disadvantages associated with the use of these metal foams, as reported previously by Detsi et al. [21]: As major advantage, a nickel foam with its high intrinsic electrical conductivity can successfully act as effective 3D bulk current collector for the electro-catalyst deposited onto its pore walls. In addition, the porous architecture of open cell nickel foams favors an effective transfer of ionic species and gas molecules at the catalyst/electrolyte interface [21]. The primary disadvantage of using commercially available nickel foams for these types of applications corresponds to the very large pore sizes of macro-foams, which is commonly in the submillimeter to millimeter range [21]. Consequently, as pointed out in ref. [21], the specific surface area of open cell nickel foams is very low [21,63–65]. In contrast to nickel foams, 3D nanoporous structures can exhibit much larger interfacial surface areas, since the specific surface area scales inversely with the average pore size [21,34,66,67]. Detsi et al. used dealloying to produce a high-performance, robust, and ultrafine mesoporous NiFeMn metal/metal oxide water oxidation electro-catalysts with average ligament size on the order of ~10 nm, BET surface area of 43 m^2/g and high

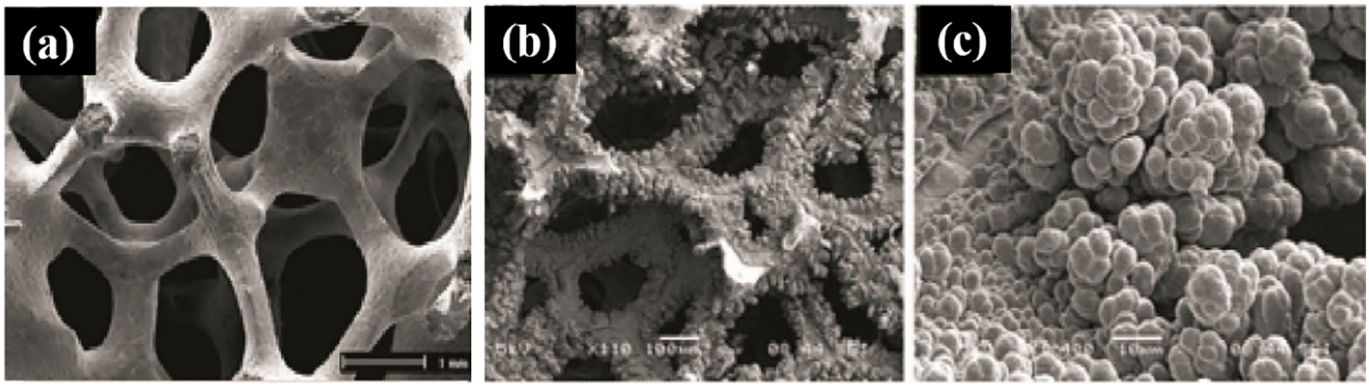

Fig. 2. (a) Open cell aluminum foam, (Reproduced from [54]). (b, c) Open-cell nickel foam coated with cobalt-based water oxidation electro-catalyst at low and high magnification, respectively.
(Reproduced from [52])

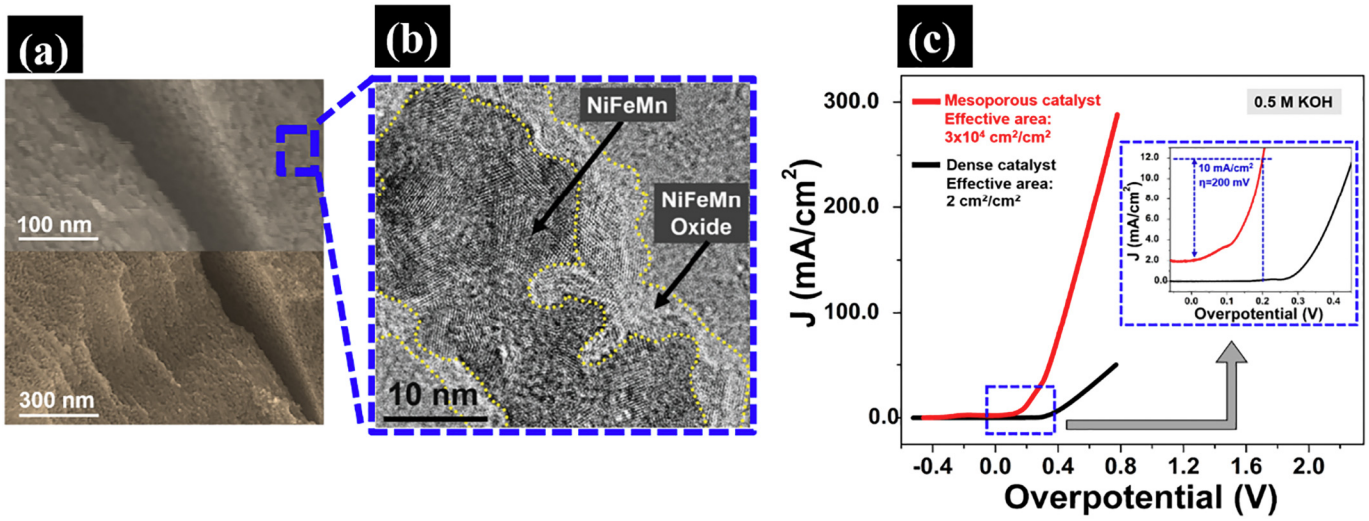

Fig. 3. (a) SEM of the fracture cross-section of a 300 mm-thick nanoporous NiFeMn-based electro-catalyst. (b) TEM showing a typical ligament in the NiFeMn-based electro-catalyst. The ligament is covered with a few nanometer-thick oxide layer as illustrated by the dashed yellow line. (c) Linear sweep voltammograms obtained from the nanoporous NiFeMn metal/metal-oxide catalyst (red) and a dense NiFeMn catalyst counterpart (black) at a sweep rate of 1 mV s^{-1} in 0.5 M KOH. The nanoporous catalyst delivers 10 mA cm^{-2} at only 200 mV (inset), while the dense catalyst counterpart does not achieve 10 mA cm^{-2} until 430 mV (sweep rate of 1 mV s^{-1}; 0.5 M KOH). (For interpretation of the references to colour in this figure legend, the reader is referred to the web version of this article.) (For interpretation of the references to colour in this figure legend, the reader is referred to the web version of this article.)
(Reproduced from ref. [21]).

electrical conductivity [21]. This was achieved by partial removal of Mn from Mn-rich ternary alloys with composition $Ni_{15}Fe_{20}Mn_{65}$ at.%.

The typical microstructure of the dealloyed ternary material with final composition $Ni_{60}Fe_{30}Mn_{10}$ at.% is shown in Fig. 3a at low and high magnifications. A mixed native oxide (i.e. Ni oxide, Fe Oxide and Mn oxide) covers the internal surface of this mesoporous alloy as depicted by the high-resolution transmission electron microscopy (TEM) image of Fig. 3b. This NiFeMn mixed oxide acts as electro-catalyst for water oxidation. Furthermore, electrons generated during water oxidation on this oxide nanocoating are effectively collected by the inner NiFeMn metallic component of this metal/metal oxide composite system. The unique combination of small ligaments and pores size (~10 nm), high BET surface area (43 m^2/g), open porosity for effective mass transfer at the catalyst/electrolyte interface, high bulk electrical conductivity for effective current flow through the electro-catalyst, makes it possible to use unprecedented thick films (~300 μm) with a high density of active catalyst sites per unit electrode area, resulting in very high current densities during water oxidation as shown in Fig. 3b, reproduced from [21]. For the sake of illustration, common unsupported non-precious metal oxygen-evolution catalysts require at least ~350 mV overpotential to oxidize water with a current density of 10 mA/cm^2 in 1 M alkaline solution. The nanoporous NiFeMn/NiFeMn oxide composite made by selective alloy corrosion exhibits an electro-catalytic activity toward water oxidation of 500 mA/cm^2 at 360 mV overpotential and is stable for over eleven days in 1 M KOH [21].

Zhang and co-workers also used the dealloying strategy to derive a high-performance mesoporous NiFe-based water oxidation electro-catalyst (see Fig. 4) during selective removal of Al from $Al_{97}Ni_xFe_{3-x}$ alloys [68]. Their composite material required only ~244 mV overpotential to oxidize water with a current density of 10 mA/cm^2 in 1 M alkaline solution [68].

Sun and co-workers used dealloying to produce high-performance NiFeCu-based metal/metal oxide water oxidation electro-catalysts during partial removal of Cu from co-deposited Cu-rich NiFeCu ternary alloys with elemental ratio Ni:Fe:Cu to be 10:1:21 [69]. The corresponding metal/metal oxide nanocomposite structure (with metallic core and oxide shell) required only ~180 mV overpotential to oxidize water with a current density of 10 mA/cm^2 in 1 M alkaline solution [69].

3.3. Critical remarks

The use of non-precious elements such as Ni and Fe in high-performance water oxidation heterogeneous nanoporous catalysts is very attractive for large scale applications. The fact that these catalysts are composite materials in the form of metal/metal oxides prevent the nanoporous metal scaffold from coarsening during water oxidation onto the oxide coating. Although ultra-small pores (e.g. ~10 nm from the structure in Fig. 3a) are needed for high specific surface areas, it is expected that during water oxidation, O_2 gas produced in the bulk of thick nanoporous catalysts (e.g. the ~300 μm thick nanoporous film from ref. [21]) will not easily escape from this bulk. A build-up of O_2 gas inside the bulk of the electrode material is susceptible to increase the internal resistance of the system, which in turn will increase the overall water oxidation overpotential. A possible solution to this problem is the design of hierarchical nanoporous electro-catalyst, where macro- and mesopores coexist. The mesopores will then provide the large surface area needed for the water oxidation reaction, while the macropores will allow O_2 gas to escape from the bulk. To our opinion, such an architecture with bimodal porosity represents the “ideal” material design.

4. Methanol oxidation

4.1. Motivation and background

Due to their high efficiency and environmental-friendliness, fuel cells have gained increased attention in the field of electrochemical energy storage and conversion [70,71]. Among these, direct methanol fuel cells (DMFCs) have the advantage of simple operation and high energy density, and thus applicable in automobile and portable electronics [23]. The methanol oxidation reaction (MOR) is critical in DMFCs, and (electro-)catalysts are required to enhance the kinetics of this reaction. The most common electro-catalysts are Pt-based materials [72,73]. However, Pt-based catalysts suffer from poisoning by CO. In addition, there are intermediates during the methanol oxidation, which causes low efficiency [74,75]. Therefore, it is necessary to find alternative catalysts that do not have such drawbacks while displaying high catalytic activities and good stability.

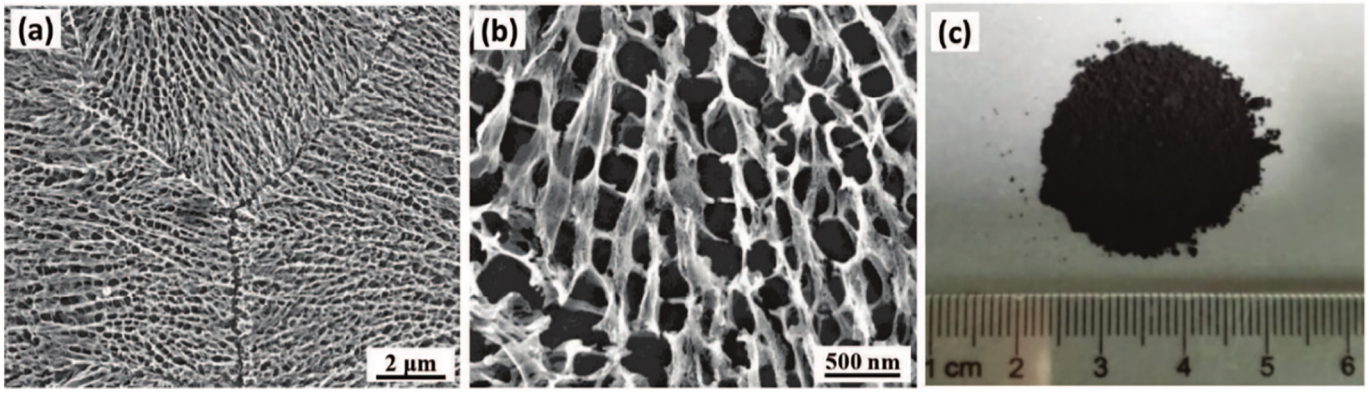

Fig. 4. (a, b) SEM images of the $Al_{97}Ni_2Fe_1$ alloy ribbon after being immersed in the 1 wt% HF aqueous solution for 8 min. (c) Photograph of the as-dealloyed Ni_2Fe_1-O powders.
(Reproduced from ref. [68])

4.2. Nanoporous gold

NP-Au has been explored as metal oxidation electro-catalyst. A typical cyclic voltammograms (CV) of NP-Au in 0.5 M KOH solution with and without 1 M CH_3OH, as reported by Ding and co-workers is shown in Fig. 5 [20]. It can be seen that the electrochemical current is significantly enhanced upon addition of methanol in the electrolyte [20]. In other words, NP-Au electrode is highly active toward methanol electro-oxidation or electro-reduction.

It was reported that electro-oxidation of methanol happens at two potential regions, namely −0.5 to 0.4 V (vs SCE) and 0.44 to 0.8 V (vs SCE), based on different mechanisms [20]. At lower potentials, four-electron transfer reaction happens [76,77]:

$$CH_3OH + 5OH^- \rightarrow HCOO^- + 4H_2O + 4e^- \quad (1)$$

while six-electron transfer process happens at higher potentials and methanol is oxidized into carbonates [76,78]:

$$CH_3OH + 8OH^- \rightarrow CO_3^{2-} + 6H_2O + 6e^- \quad (2)$$

The four-electron process (Eq. (1)) takes place in combination with both the chemisorbed OH^- and the formation of pre-oxidation species [20,76,78]. As potential reaches −0.5 V, OH^- anions start to chemisorb on the NP-Au surface, which onsets the methanol oxidation process; As the potential sweeps positively, more OH^- will adsorb on the NP-Au surface and react with gold surface atoms to form "pre-oxidation precursors" such as Au-$OH_{ads}^{(1-m)-}$, where "m" is the charge-transfer coefficient that varies between 0 and 1 [20,78].

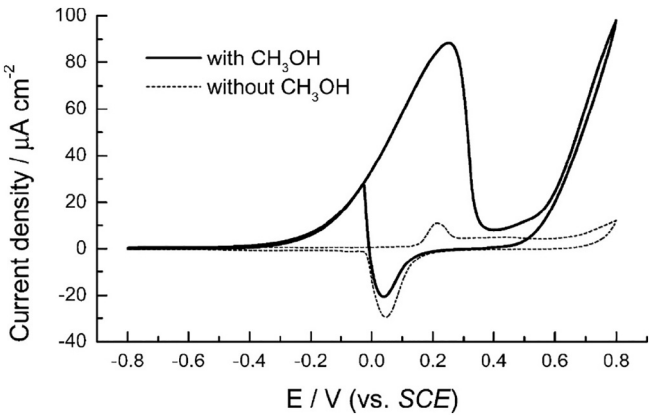

Fig. 5. Cyclic voltammograms (CVs) of NP-Au electrodes in 0.5 mol dm^{-3} KOH solutions with and without 1.0 mol dm^{-3} CH_3OH. The potential scan rate was 10 mV s^{-1}.
(Reproduced from ref. [20]).

This partially oxidized NP-Au will greatly enhance the oxidation of methanol, as shown in the first peak in Fig. 5 [20]. However, as potential increases, Au-$OH_{ads}^{(1-m)-}$ will be consumed to form relatively dense and ordered gold oxides, and the exhaustion of Au-$OH_{ads}^{(1-m)-}$ will slow down and eventually stop the methanol oxidation reaction [20]. Thus, an inhibition to the methanol oxidation initiates at around 0.25 V (vs SCE), as can be seen from Fig. 5 [20]. At more positive potentials, the methanol oxidation reaction is again activated through those earlier formed gold oxides [79]. Herein the six-electron transfer reaction happens (Eq. (2)), providing an alternative reaction channels for methanol oxidation [20]. It also allows reaction intermediates produced at lower potentials to be further oxidized, thus eliminating potential catalyst poisoning [20]. This is a great advantage over Pt-based material. Also, the oxidation was observed to occur at less positive potentials, which agrees with the work of Borkowska et al. [80].

As potential sweeps negatively, first there will be electrochemical reduction of gold surface oxides corresponding to a reduction peak at around 0.04 V (vs SCE) [20]. With the removal of oxide, Au-$OH_{ads}^{(1-m)-}$ is recovered and initiating four-electron oxidation process at around 0 V (vs SCE) [76,78]. Although Ding and co-workers found the greatly enhanced catalytic activity of NP-Au for methanol oxidation, they also observed the decrease in activity upon long-time cycling [20].

Since there is no catalyst poisoning, this decrease should be attributed to the change of surface structure [20]. As shown in Fig. 6, the starting NP-Au has an average pore/ligament size around 12 nm, while after cycling it seriously coarsens to more than 40 nm. They have concluded that the coarsening and clogging of pores result in the loss of active surface area, which in turn decrease the electro-activity of NP-Au [20].

Weissmüller and co-workers [81] held two doubts upon re-examination the results of Zhang et al.: (1) The conclusion of the six-electron reaction product carbonate (CO_3^{2-}) was based on assumptions for planar electrodes during ethanol oxidation [76,77], and was not supported by experimental evidence. (2) The performance of NP-Au as an electro-catalyst compared to other porous gold materials with different activities [74,82,83] is unknown.

It is suggested that NP-Au properties vary with the dealloying techniques [84], which result in different surface structure [85] and surface-located Ag clusters [86]. Therefore, Weissmüller and co-workers prepared three types of NP-Au, namely through mild and harsh potentiostatic dealloying as well as open-circuit corrosion [81]. Fig. 7 shows the scanning electron microscopy (SEM) images of the three type NP-Au, and the corresponding sample properties are summarized in Table 1 [81].

As can be seen from Table 1, NP-Au (A) has the smallest pore/ligament size that corresponds to the highest surface area [81]. It is known that small pores and ligaments feature a higher curvature [87],

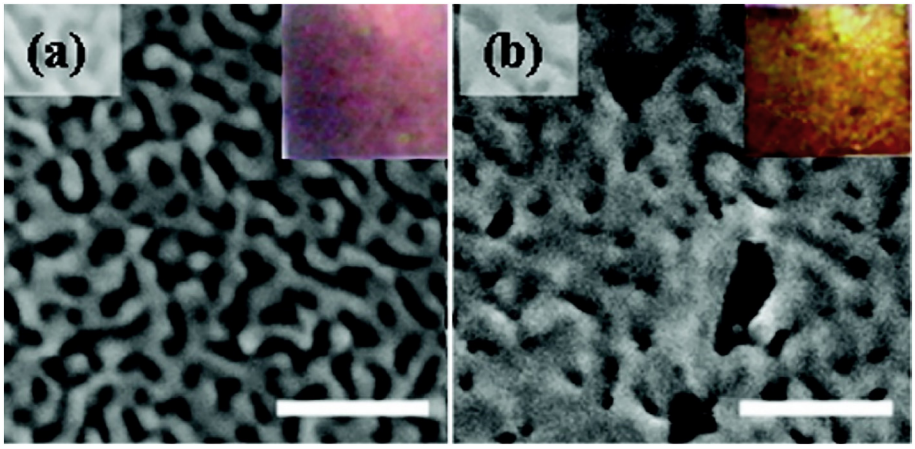

Fig. 6. SEM images of an NPG electrode measured before (a) and after (b) electro-oxidation of methanol. Scale bars in two SEM images are 100 nm. Insets in two images show the change of the colour of NPG before and after the electro-catalytic reaction.
(Reproduced from ref. [20]).

which is in turn associated with more low-coordinated atoms. Low-coordinated sites usually display higher activity [88], but the NP-Au (A) here shows the lowest current (42 μA/cm^2); On the other hand, samples with less low-coordinated sites show much higher current density (101 μA/cm^2 for NP-Au (B) and 127 μA/cm^2 for NP-Au (C)) [81]. Note that these values are within the range of previously reported results, namely 22 μA/cm^2 for Xu et al. [83], and 87 μA/cm^2 for Zhang et al. [20]. The poor activity of NP-Au (A) is attributed to the inefficient methanol saturation inside the nanopores, meaning that the smaller pores suffer more from the transport control [81].

As shown in Fig. 8 (reproduced from ref. [81]), the selectivity for HCHO decreases as residual Ag (X_{Ag}) increases. In other words, NP-Au (A) promotes four-electron transport process (Eq. (1)) over two-electron transport process with increasing X_{Ag} [81].

However, the authors found that indeed X_{Ag} and selectivity is not directly connected [81]. Instead, since X_{Ag} and bulk ligament size (L_B) are interrelated such that smaller ligaments contain more Ag [84], more residual Ag results in an increased transport limitation. Thus, the fast-interfacial reaction, i.e. the two-electron oxidation to HCHO [89] is more strongly affected than the slower four-electron oxidation to $HCOO^-$ [81]. Note that the authors here did not find carbonate as a product [81].

Methanol can also be oxidized to methyl formate in the presence of O_2. Wittstock et al. showed that for stoichiometric compositions of methanol and O_2, under room temperature the selectivity to methyl formate is almost 100% with 10% conversion of methanol [19]. Upon increasing the temperature to 80 °C, the conversion increases to 60% while remaining high selectivity (97%) [19].

Model studies [90] reveal that methanol is activated by surface oxygen, and will be eventually oxidized to CO_2 if O_2 is in excess. The mechanism is shown in Fig. 1a above. This work is indicative since the product here, namely methyl formate, is the precursor for formic acid, formamide and dimethyl formamide, and thus embraces various applications [91].

In addition to using pure NP-Au as catalyst, hybrid material systems such as Pt/NP-Au catalyst also exhibit high performance over methanol electro-oxidation. Ding and co-workers obtained excellent performance toward methanol and CO oxidation using Pt-decorated NP-Au leaf in acidic solutions [92]. Similar result was obtained by Zhang et al., where Pt/NP-Au catalyst displays more negative onset potential for methanol oxidation as well as significantly enhanced current density [20]. This may shed light on possibilities for alternative ultralow precious metal loading catalyst to traditional ones, and is promising in green-energy applications [92].

4.3. Nanoporous palladium

Zhang and co-workers obtained a novel structure, namely nanoporous palladium (NP-Pd) rod (see Fig. 9) through dealloying of Pd-Al alloy in acid [93].

It was loaded onto a freshly polished glassy carbon as a catalyst for methanol electro-oxidation [93]. Cyclic voltammetry (CV) shows two anodic peaks, one at positive potential sweep and the other at negative potential sweep, respectively (Table 2) [93]. The peak located in the positive scan is correlated to the oxidation of chemisorbed methanol molecules [94–96]. The negative scan peak is attributed to methanol oxidation after Pd surface oxide is reduced [93,97], same scenario as methanol oxidation using NP-Au [20]. Similar CV trend, as well as greatly enhanced catalytic activity is also observed with NP-Pd obtained from Pd-Al alloy in basic solution [98].

As can be seen from Table 2, the relation between NP-Pd mass loading and peak current density is not linear [93]. It indicates that there is an optimal metal dispersion ratio in the carbon matrix, which will result in largest electrochemical active surface area (EASA) [93]. When the mass loading exceeds the optimal ratio, metal particles agglomerate and reduce the amount of three-phase reaction interface, thus catalytic activity decreases [93]. Similar trend is also observed for other material systems [99,100].

4.4. Critical remarks

Up to now, various nanostructured materials have been investigated as potential candidates for high-performance methanol oxidation catalysts. Conventional approaches include the use of nanoparticles supported on conductive substrate such as carbon-supported Au-Pt nanoparticles [101–103]. One potential drawback of using such approach originates from the difficulty of achieving effective particle dispersion: various surface chemistry techniques are necessary for nanoparticles to be uniformly dispersed within the conductive support matrix, and during such surface modification process it is possible to cause structural damage to the support, leading to loss of conductivity and thus lowering the performance [104,105]. On the other hand, nanoporous metal catalysts are self-supported, with good conductivity and mechanical stability, thus eliminating the risk of having conductive support lowering the overall catalytic activity.

The 3D NP-Au and NP-Pd electro-catalysts have the advantage of effectively suppressing poisoning from CO during methanol oxidation, which is otherwise the main drawback of using Pt-based catalysts. Although they display high electro-catalytic performance, the porous structure of metal will eventually coarsen in aqueous solutions, which

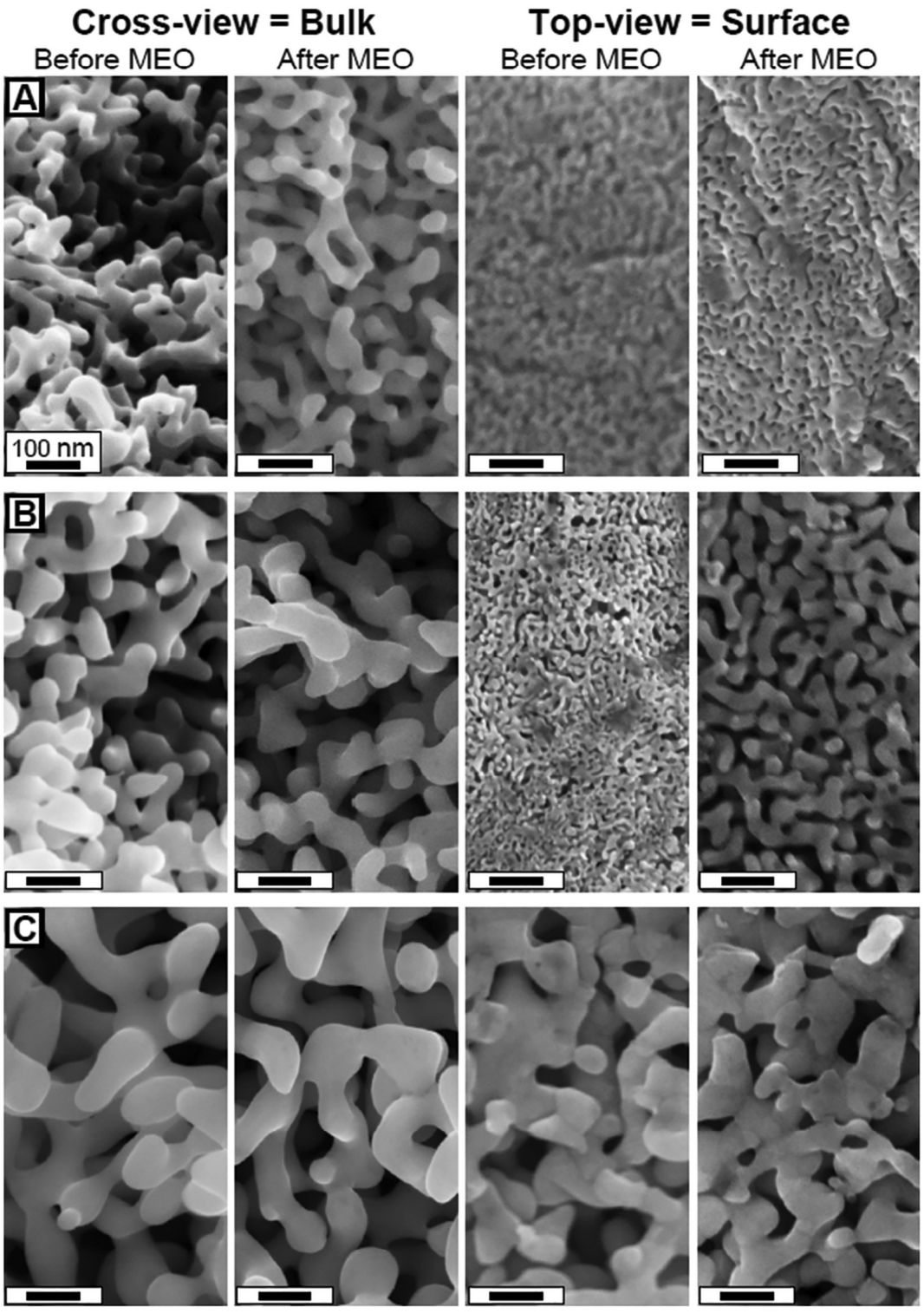

Fig. 7. Scanning electron micrographs of NP-Au samples prepared by A: potentiostatic dealloying in $HClO_4$, B: potentiostatic dealloying in HNO_3 and by C: open-circuit dealloying in HNO_3. Left two columns: cross-sections after sample cleavage. Right two columns: top-views onto the flat sample surface. Cross-views and top-views refer to the state after dealloying (first and third column) and after ten cyclic voltammetry scans in 1 M KOH + 1 M CH_3OH (second and fourth column). All scale bars: 100 nm.
(Reproduced from ref. [81]).

results in the decrease of active surface area and therefore poses a challenge for long-term cycling stability [20]. In addition, the pore size should be controlled within an optimal range where mass transport can be effectively facilitated [81]. Otherwise the overall performance could be limited by mass transport. Last but not least, the high cost of material is also a limiting factor for large scale applications.

Table 1
Properties of NP-Au and Au electrode.

	NP-Au (A)	NP-Au (B)	NP-Au (C)	Au
L_B (nm)[a]	28	51	69	–
	34	46	67	–
L_s (nm)[a]	8	9	58	–
	16	26	58	–
$X_{Ag\text{-}EDX}$ (at.%)[a]	3.6	0.1	0.8	–
	4.7	0.2	0.3	–
$X_{Ag\text{-}XPS}$ (at.%)[a]	15.0	16.1	6.7	–
	14.4	9.1	7.2	–
C (mF)	48.6	32.2	6.4	0.2
A (cm^2)	1216.2	805.0	161.0	5.2
A_m (m^2/g)	7.2	4.7	1.0	0.003
I_p/A ($\mu A/cm^2$)	(1st) 42.0	101.1	119.4	73.8
	(10th) 38.4	92.3	109.8	–
E_p (mV)	(1st)550	532	420	280
	(10th) 504	507	403	280
C_{HCHO} (μM)	75.2	303.4	87.9	236.4
C_{HCOO^-} (μM)	2613.0	4095.9	938.4	1288.3

[a] Two values are provided with upper ones corresponding to values before MEO (methanol oxidation) and lower ones after MEO.

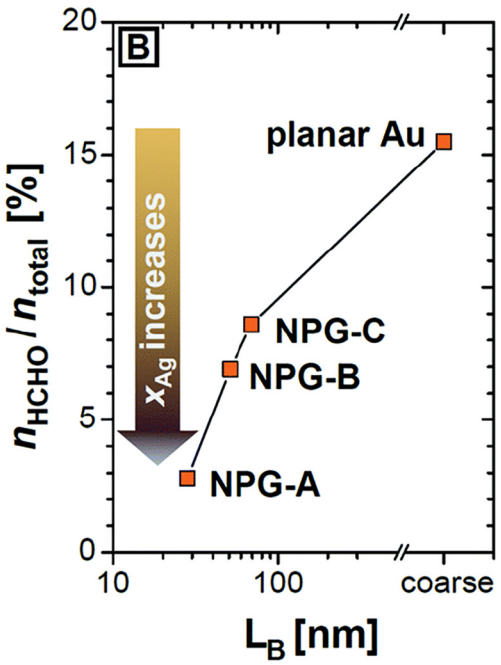

Fig. 8. Fraction of HCHO on the total product amount (HCHO + $HCOO^-$) in dependence on the bulk ligament size, L_B. The corresponding increase of x_{Ag} (from EDX and XPS after cycling) is indicated by the arrow.
(Reproduced from ref. [81])

5. Carbon dioxide reduction to carbon monoxide

5.1. Motivation and background

It goes without saying how essential it is to bring down the concentration of the CO_2 greenhouse gas [24,25]. This can be achieved through electrochemical reduction of CO_2 into other reusable carbon fuels such as CO and CH_4 [26–29]. However, CO_2 is a fully oxidized and one of the most stable molecule among carbon-based substances [30,31]. For example, the formation of its first reduction reaction intermediate, namely CO_2^-, in aqueous solution requires up to −1.9 V vs standard hydrogen electrode (SHE) [30,32]. This very negative potential creates high thermodynamic energy barrier as well as sluggish kinetics for overall reduction process. Thus, it brings us the challenge of how to develop a cost effective, high selectivity and high efficiency catalyst that can function in aqueous solution [106].

Aside from the various potential reduction products of CO_2, herein we focus on CO_2 reduction to CO, which is one of the reduction pathways that attracts most attention and is a promising route for clean energy [17]. It is demonstrated that among noble metals, Au and Ag have the highest catalytic activities for CO_2 reduction to CO [30]. To further improve the performance, recent research has been devoted to developing various nanostructured electro-catalysts, which demonstrate not only huge surface reactive area but also enhanced intrinsic activity [107–112]. Here, we illustrate how nanoporous Ag and Au can be used as highly selective efficient catalyst for CO_2 reduction to CO in aqueous media, while highlighting the advantages of nanoporous structure over the other nanostructured materials.

5.2. Mechanism of electrochemical reduction of carbon dioxide to carbon monoxide

The overall reduction reaction of CO_2 to CO is stated in Eq. (3) [30]. The potential value is estimated from thermodynamic data in aqueous media at 25 °C [113].

$$CO_2 + H_2O + 2e^- \rightarrow CO + 2OH^-(-0.52V \text{ vs SHE}) \quad (3)$$

It is commonly accepted that the above reduction process on metal surfaces can be divided into two steps, with the initial step being one-electron transfer to form adsorbed CO_2^- (Eq. (4)) [18]:

$$CO_2 + e^- \rightarrow CO_{2ads}^- \quad (4)$$

The standard reduction potential for the CO_2/CO_{2ads}^- couple is very negative (−1.9 V vs SHE) [30,114], meaning that in most cases (i.e. for polycrystalline metal film) the initial step is acting as the rate determining step. However, this can be shifted to more positive values if there are specific interactions between the adsorbed CO_2^- radical and the surface atoms of the metal electrode [18,115]. The second step is the reaction intermediate CO_{2ads}^- with two protons and another electron to form the final product CO. This can be further divided into three sub-sequential steps [18,116]:

$$CO_{2ads}^- + HCO_3^- \rightarrow COOH_{ads} + CO_3^{2-} \quad (5)$$

$$COOH_{ads} + HCO_3^- + e^- \rightarrow CO_{ads} + H_2O + CO_3^{2-} \quad (6)$$

$$CO_{ads} \rightarrow CO \quad (7)$$

Eq. (5) is a chemical step involving protonation of CO_{2ads}^- to form $COOH_{ads}$ intermediate [117]. Herein HCO_3^- acts as the proton source since it has much lower pK_a than water [116]. Eqs. (6) and (7) are the processes associated with the formation of final product and its desorption [18].

5.3. Nanoporous silver

Among various metal catalysts, silver is one of the most investigated and promising material due to its excellent CO_2 to CO selectivity (above 80%) along with relatively reasonable cost [30,118]. In addition, due to its all-inorganic nature, it is expected to be more stable under harsh catalytic environments than homogeneous catalysts [17,119,120]. Recently, several silver-based nanostructured electro-catalysts with enhanced performance have been developed under various experimental conditions [106,121]. Herein, we focus on introducing nanoporous silver (NP-Ag) as an efficient and highly selective catalyst for CO_2 to CO conversion. NP-Ag can be obtained through different methods. De-Hosson and co-workers reported on the fabrication of ultrafine NP-Ag with structure size in the range of 30 nm by selective removal of Al from non-equilibrium (i.e. quenched) single-phase Ag/Al parent alloys [34]. Lu et al. [17] used this procedure to fabricate NP-Ag with ligament size ~50–200 nm for CO_2 reduction (Fig. 1b). Deng et al. [122] studied the tunability of pore size using catalytically driven reaction. Hsieh et al.

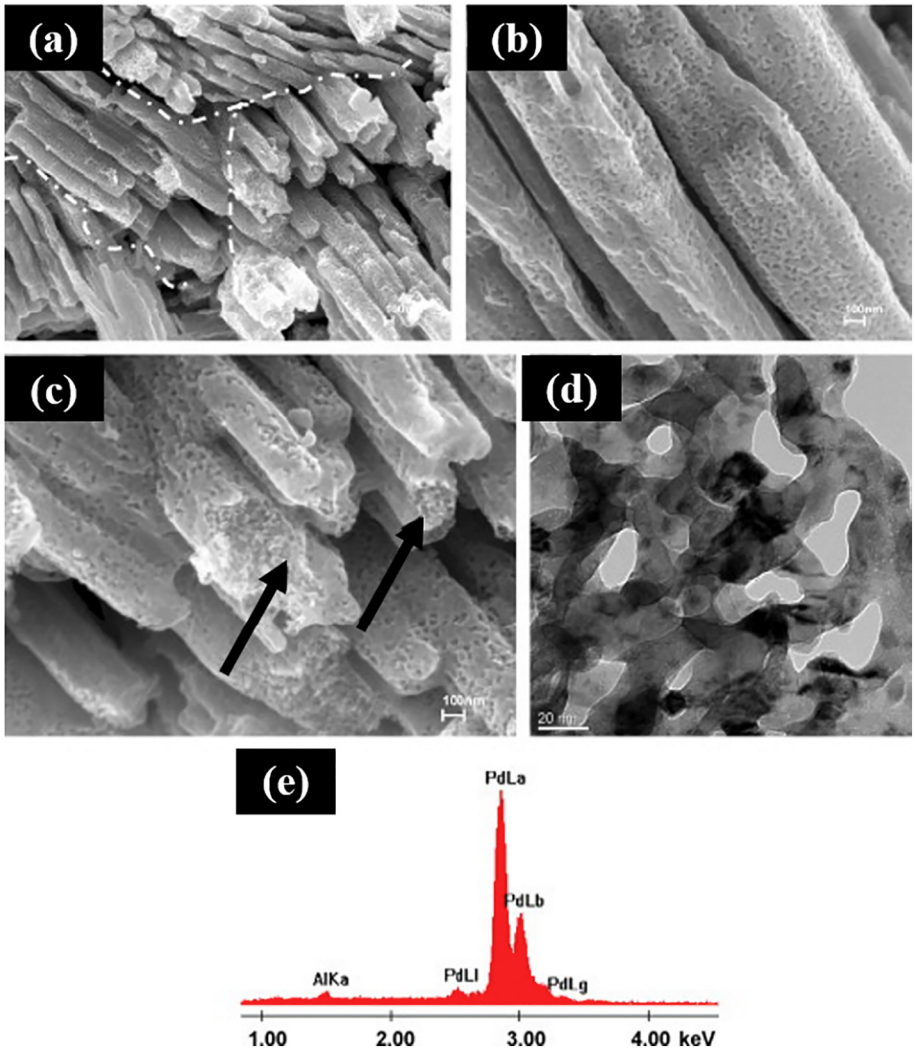

Fig. 9. (a–c) SEM and (d) TEM images showing the microstructure of the NP-Pd rods through chemical dealloying of the $Al_{80}Pd_{20}$ alloy in the 5 wt% HCl solution. (e) EDX spectrum showing the composition of the NP-Pd rods.
(Reproduced from ref. [93])

Table 2
CV parameters for methanol oxidation on NP-Pd rods.

NP-Pd rods loading (mg/cm^2)	E_{op} (mV)	Positive scan		Negative scan	
		j_p (mA/mg)	E_p (mV)	j_p (mA/mg)	E_p (mV)
0.2	−404	166.94	−80	89.49	−143
0.4	−401	223.52	−42	146.18	−123
0.6	−400	208.20	−22	129.30	−117
0.8	−392	129.22	−28	104.74	−109
1.0	−390	118.61	−17	113.47	−89
1.2	−367	99.68	−22	90.01	−89

[18] used oxidation-reduction method in the presence of chloride anions for NP-Ag fabrication (Fig. 10). Yoon et al. [123] prepared mesostructured Ag inverse opals (Ag-IO) by replication of colloidal polystyrene thin films on Au-coated glass slides. Note that this fabrication process is "selective leaching" of templates but not a typical dealloying process [123]. The Ag-IO exhibits uniform surface structure, porosity and tortuosity (Fig. 11) [123]. Those porous structure was found to exhibit exceptional activity, not only due to the extreme increase in surface area for catalytic reaction, but also resulting from creation of highly curved internal surface which contains highly active step sites for CO_2 conversion [118].

The performance of NP-Ag catalyst is tested in CO_2-saturated $KHCO_3$ electrolyte under various overpotentials. Gas-phase products are collected and analyzed using gas chromatography (GC). Greatly enhanced Faradaic Efficiency (FE) is observed under low overpotentials, along with modified selectivity and cycling stability [17,18] (Figs. 12 and 13). The performance of NP-Ag catalyst is also compared with that of Ag-foil and other Ag nanostructures as potential CO_2 electro-catalysts [17] (Table 3). It is demonstrated that NP-Ag exhibits significant advantages over other types of silver catalysts under aqueous environments in both overall and per surface site activity [17].

Tafel analysis is performed to further explore kinetics of CO_2 reduction on the NP-Ag catalyst surface (Fig. 14) [17]. For Ag foil (polycrystalline Ag) it has an Tafel slope of 132 mV dec^{-1}, which is close to the theoretical value (118 mV dec^{-1}) and the value (~140 mV dec^{-1}) obtained under similar experimental conditions [17,18,30,124,125]. This indicates that for Ag foil the rate determining step is CO_2 gaining an electron to be CO_2^- [17]. For NP-Ag, on the other hand, the Tafel slope of 58 mV dec^{-1} indicates that it has a fast electron transfer step, followed by a non-electron transfer rate-determining step [17,126]. This further confirms that NP-Ag surfaces are better in stabilization of CO_2^- intermediate [17]. Similar results have been reported for Ag system [18] (Fig. 15) as well as other systems [124]. It is also suggested that for NP-Ag, the real rate-determining step is the

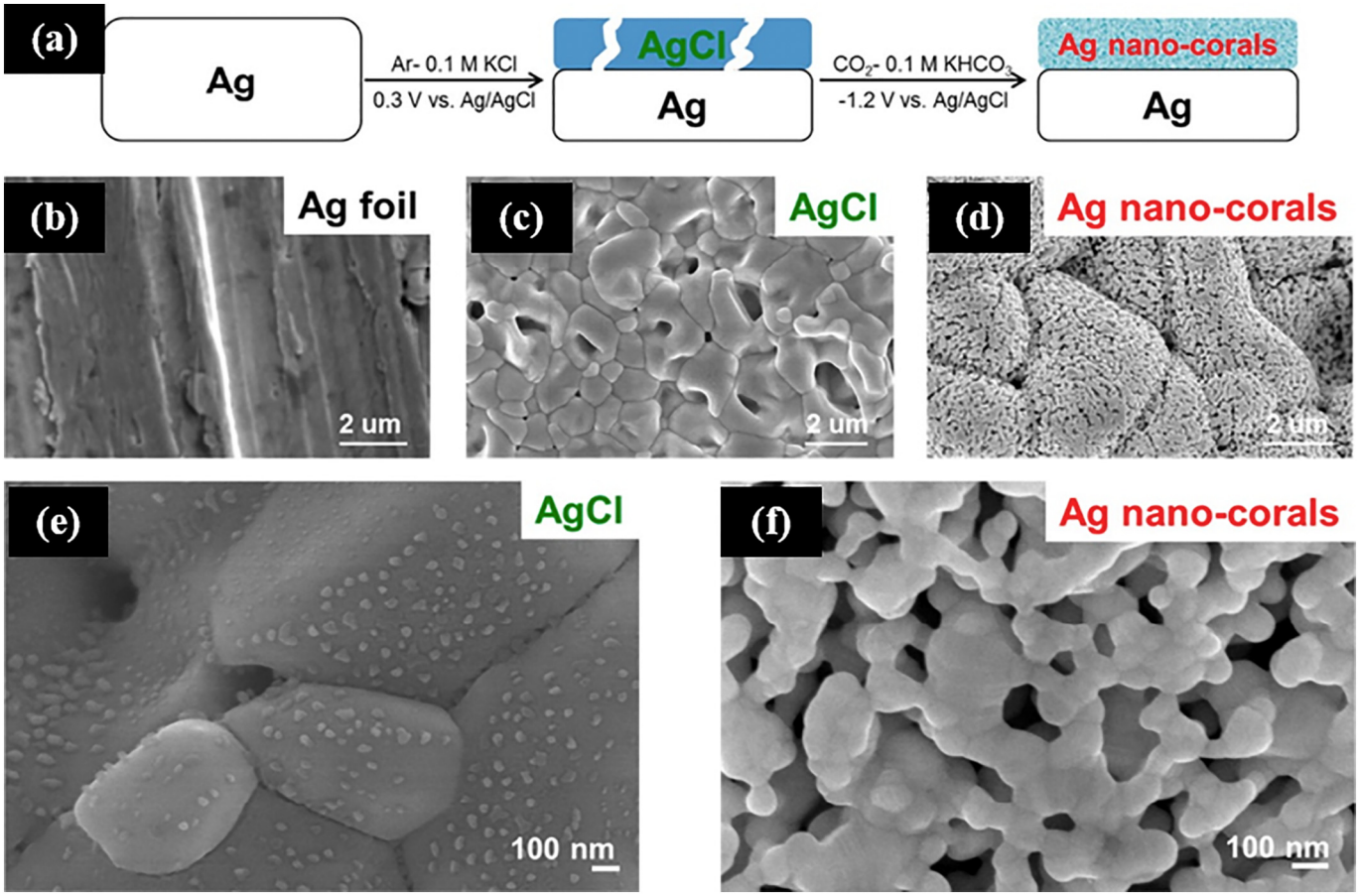

Fig. 10. (a) Schematic illustration of the formation of as-prepared AgCl and Ag nanocorals. SEM images of (b) untreated Ag foil, (c) as-prepared AgCl after 12 h oxidation, and (d) Ag nanocorals. High-magnification SEM images of (e) as-prepared AgCl after 12 h oxidation and (f) Ag nanocorals.
(Reproduced from ref. [18])

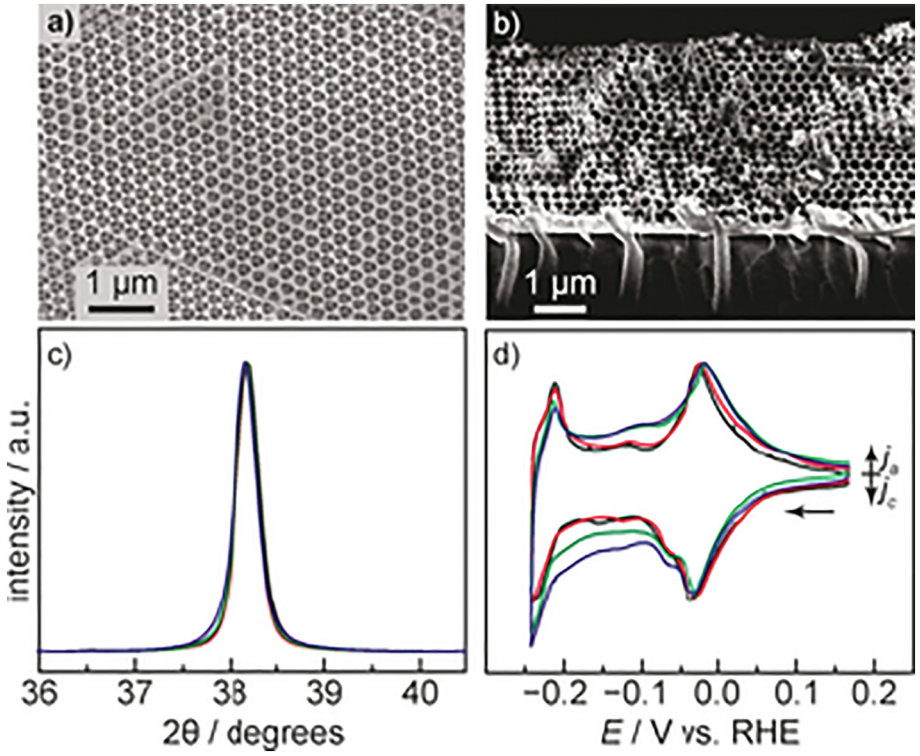

Fig. 11. (a) Top down (b) and cross-sectional SEM images of a Ag-IO film prepared by passing a 1 C cm^{-2} Ag deposition charge. (c) Normalized X-ray diffraction peak for the Ag (111) reflection and (d) normalized cyclic voltammograms of thallium UPD and stripping for nominally planar Ag films (black) and Ag-IO samples prepared by passing of 0.5 C cm^{-2} (red), 1 C cm^{-2} (green), and 2 C cm^{-2} (blue) Ag deposition charges. Voltammograms were normalized with respect to the −0.03 V peak. (For interpretation of the references to colour in this figure legend, the reader is referred to the web version of this article.) (For interpretation of the references to colour in this figure legend, the reader is referred to the web version of this article.)
(Reproduced from ref. [123])

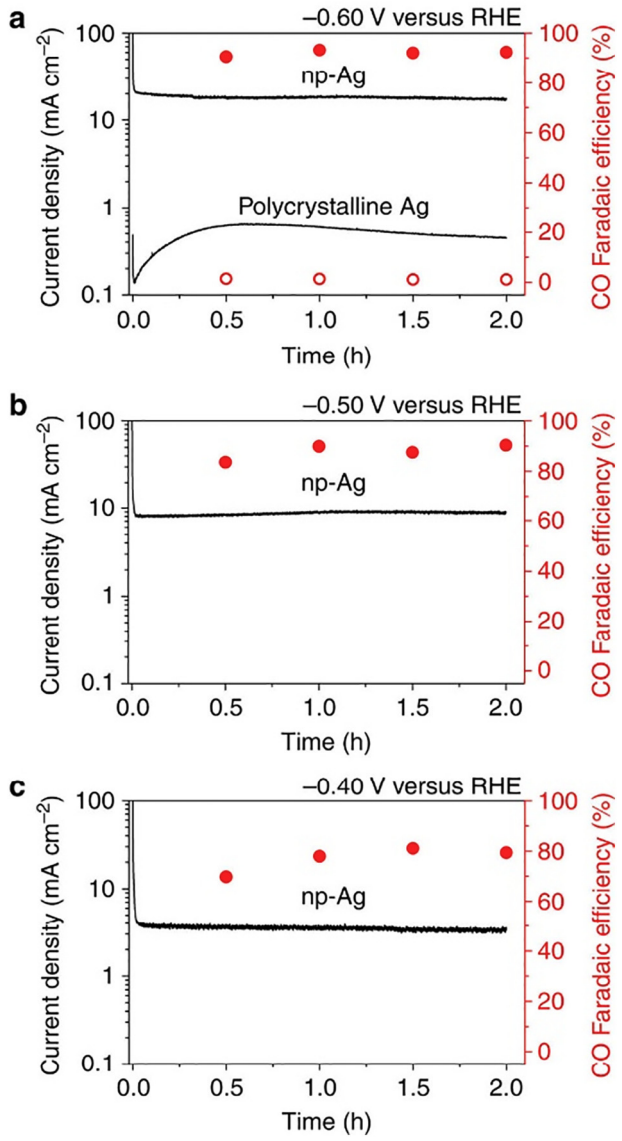

Fig. 12. Electro-catalytic performance of NP-Ag. CO_2 reduction activity of NP-Ag and polycrystalline silver at (a) −0.60 V, and NP-Ag at (b) −0.50 V and (c) −0.40 V versus RHE. Total current density versus time on (left axis) and CO Faradaic efficiency versus time (right axis).
(Reproduced from ref. [17])

migration of HCO_3^- to the surface sites inside the pores of NP-Ag, where HCO_3^- is acting as proton donor for the second electron transfer process [17]. In addition, it is demonstrated that NP-Ag displays a higher intrinsic activity over polycrystalline Ag, which may result from the fact that the NP-Ag catalyst contains a higher density of step sites with possibly higher-index facets supported by the highly curved surface [127,128], and the presence of halides (i.e. chloride ion) on the Ag electrode surface or in the proximity of the solid-solution interface will further promotes the selectivity and activity of the CO_2 electro-reduction reaction [18].

5.4. Nanoporous gold

Gold is the most active catalyst for CO_2 reduction to CO among common metals, operating at the lowest overpotential and displaying high selectivity (~87%) [30]. However, due to its high material cost and low abundance it is not suitable for large-scale applications. Several works focusing on reducing CO_2 to CO using gold nanoparticles (Au-

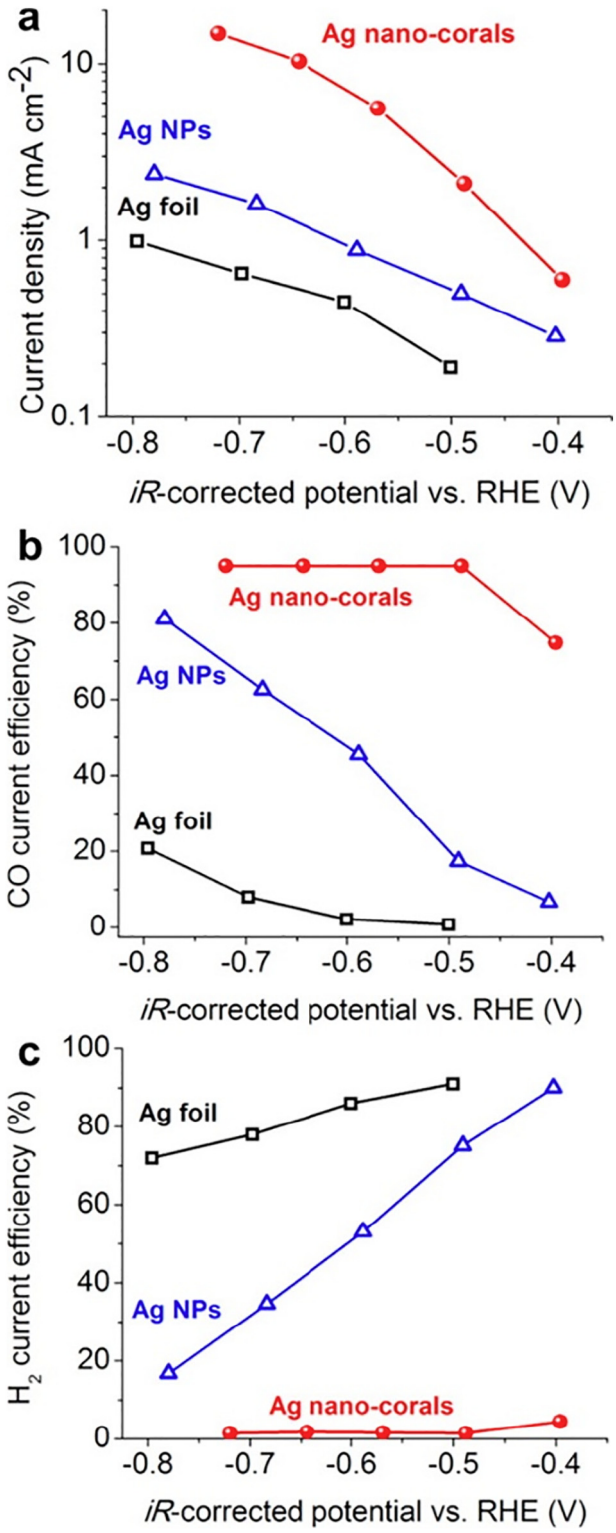

Fig. 13. (a) Total current density, (b) CO current efficiency, and (c) H_2 current efficiency, measured in CO_2-saturated 0.1 M $KHCO_3$ at different potentials (iR-corrected), for Ag foil (hollow black square), Ag nanoparticles (NPs, hollow blue triangle), and Ag nanocorals (red sphere). (For interpretation of the references to colour in this figure legend, the reader is referred to the web version of this article.) (For interpretation of the references to colour in this figure legend, the reader is referred to the web version of this article.)
(Reproduced from ref. [18])

Table 3
Summary of silver electro-catalysts for CO_2 reduction.

Material	Electrolyte	pH	Over-potential (mV)	j_{CO} (mA cm^{-2})	j_{CO} (mA/mg)	BET surface area (cm^2)	Electrochemical surface area (cm^2)	Cell type	Ref
Polycrystalline Ag	0.1 M $NaHCO_3/CO_2$	7.2	840	~4.1	N/A	2	N/A	A	[30]
Polycrystalline Ag	0.5 M $KHCO_3/CO_2$	7.2	490	0.005	$4.8*10^{-5}$	2	~16	A	[17]
Polycrystalline Ag	0.5 M $KHCO_3/CO_2$	7.2	390	Negligible	Negligible	2	~16	A	[17]
Ag nanowire 1 mg cm^{-2} loading	0.5 M $KHCO_3/CO_2$	7.2	390	Negligible	Negligible	~33	~37	A	[17]
Ag nanoparticle 1 mg cm^{-2} loading	0.5 M $KHCO_3/CO_2$	7.2	390	0.022	0.022	71	~69	A	[17]
Ag nanoparticle 10 mg cm^{-2} loading	0.5 M $KHCO_3/CO_2$	7.2	390	0.215	0.0215	710	~674	A	[17]
Ag nanoparticle 6.7 mg cm^{-2} loading	EMIM-BF_4	N/A	170	~0.61	0.091	N/A	N/A	B	[106]
Ag nanoparticle 6.7 mg cm^{-2} loading	EMIM-BF_4	N/A	670	~0.92	0.137	N/A	N/A	B	[106]
Ag nanoparticle 1 mg cm^{-2} loading	1 M KOH/CO_2	N/A	N/A	~1 (−1.4 V vs Ag/AgCl)	~1 (−1.4 V vs Ag/AgCl)	N/A	N/A	B	[109]
Ag pyrazole/carbon 1 mg cm^{-2} loading	1 M KOH/CO_2	N/A	N/A	~3 (−1.4 V vs Ag/AgCl)	~3 (−1.4 V vs Ag/AgCl)	N/A	N/A	B	[109]
Nanoporous Ag	0.5 M $KHCO_3/CO_2$	7.2	390	8	0.1989	2852	~2650	A	[17]

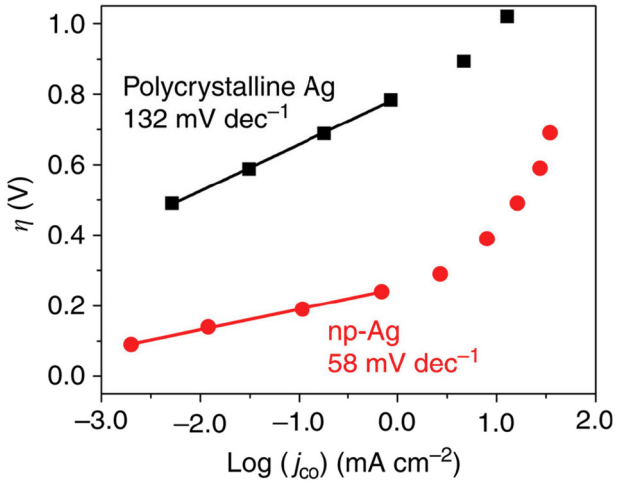

Fig. 14. Tafel analysis. Overpotential versus CO production partial current density on polycrystalline silver and NP-Ag.
(Reproduced from ref. [17])

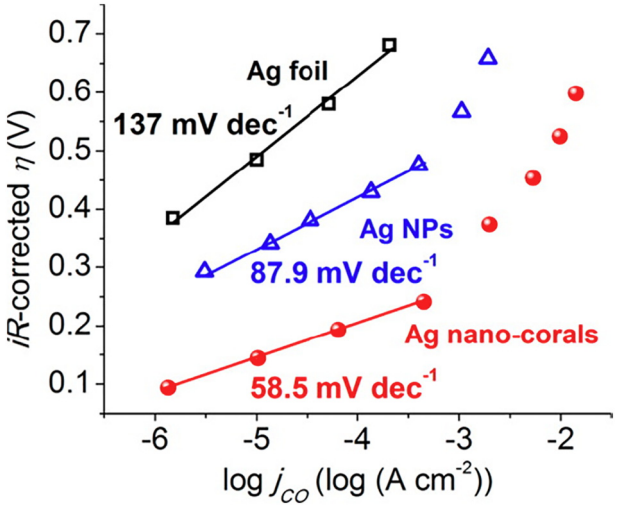

Fig. 15. Tafel plot at different overpotentials η (iR-corrected) as a function with the CO partial current density j_{CO}, on Ag foil (hollow black square), Ag NPs (hollow blue triangle), and Ag nanocorals (red sphere). (For interpretation of the references to colour in this figure legend, the reader is referred to the web version of this article.) (For interpretation of the references to colour in this figure legend, the reader is referred to the web version of this article.)
(Reproduced from ref. [18])

NP) have been reported [110,124,129]. Hall et al. reported using Au inverse opal (Au-IO) with uniform pore distribution for highly selective CO_2 to CO conversion [130]. They claimed enhanced catalytic performance with increasing porous Au film thickness, achieving 99% selectivity for CO evolution at overpotentials as low as 0.4 V [130].

The Au-IO is obtained using similar method as mentioned previously [123]. Again, it should be noted that although the nanoporous structure is obtained through selective leaching of templates, this process is different from typical dealloying defined previously [130]. SEM images suggest formation of ordered porous network extending uniformly from the surface of the film to the underlying Au substrate (Fig. 16) [130]. X-ray diffraction (XRD) and underpotential deposition (UPD) reveal similar grain structure and surface termination [130].

The increased selectivity for CO revolution over Hydrogen evolution reaction (HER) is suggested to stem from the generation of diffusional gradients within the pores [130]. It is shown that the specific activity for CO evolution displays roughly log-linear scaling versus applied

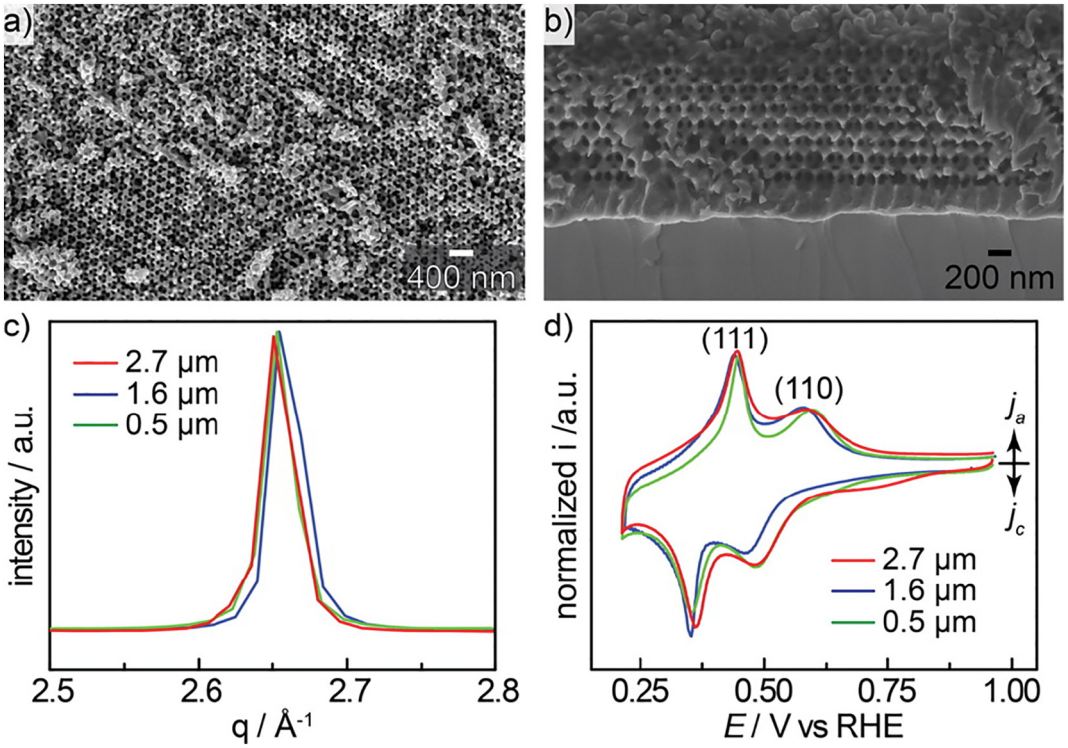

Fig. 16. Top down (a) and cross sectional (b) SEM images of Au-IO thin film. Grazing incidence XRD (c) of 0.5 (green), 1.6 (blue), 2.7 (red) μm thick Au-IO samples showing the Au (111) Bragg diffraction peak. Cyclic voltammograms (d) of 0.5 (green), 1.6 (blue), 2.7 (red) μm thick Au-IO samples recorded in 0.1 M NaOH containing 0.01 M $Pb(OAc)_2$ (10 mV s^{-1} scan rate). (For interpretation of the references to colour in this figure legend, the reader is referred to the web version of this article.) (For interpretation of the references to colour in this figure legend, the reader is referred to the web version of this article.)
(Reproduced from ref. [130])

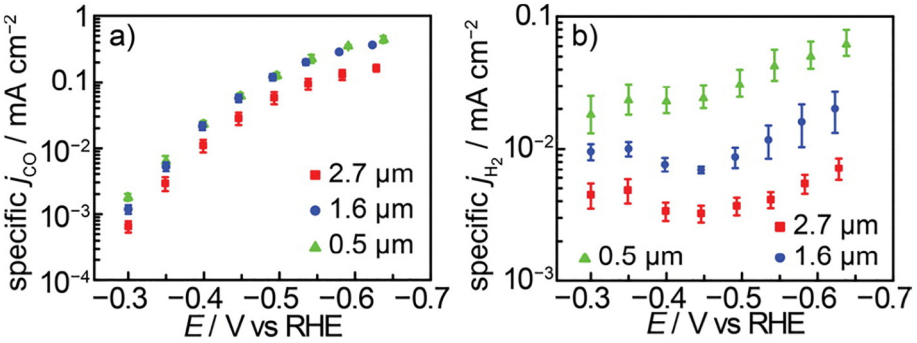

Fig. 17. Specific activity for CO (a) and H_2 (b) evolution for 0.5 (green triangles), 1.6 (blue circles), 2.7 (red squares) μm thick Au-IO samples evaluated in CO_2-saturated 0.1 M $KHCO_3$ electrolyte, pH 6.7. Error bars represent standard deviations of three independently synthesized Au-IO samples for each thickness. (For interpretation of the references to colour in this figure legend, the reader is referred to the web version of this article.) (For interpretation of the references to colour in this figure legend, the reader is referred to the web version of this article.)
(Reproduced from ref. [130])

overpotential, while the HER polarization curve is sigmoidal (Fig. 17) [130]. The decrease in the specific activity for CO evolution for the thickest sample is attributed to the onset of transport limitations [130]. Nevertheless, the inhibition of HER is principally driven by increased alkalinity that develops within the porous network during catalysis [130].

It is also suggested that this increased alkalinity serves to directly slow the rate of HER via local depletion of competent proton donors such as HCO_3^- [130]. In addition, computational and experimental data indicate that hydroxide adsorption promotes CO binding to Au [131–133]. Thus, increased alkalinity may also indirectly suppress HER through enhanced CO adsorption [130].

5.5. Critical remarks

It is demonstrated that nanoporous structures of Au and Ag not only greatly enhances the specific surface area, but also generates a large number of highly active step sites for CO_2 conversion through the curved internal surface [134]. This leads to total electro-catalytic activity even orders of magnitude higher than planer material at a moderate overpotential [134]. However, Au and Ag are not suitable for large-scale applications due to their high costs. On the other hand, some earth-abundant non-precious metal including Zn can selectively convert CO_2 into CO [134,135]. Several Zn-based nanostructured electro-catalysts with modified performance have been developed recently [134,136,137]. However, there still exists difficulty in introducing nanoporosity into Zn metal electro-catalyst through dealloying due to the highly reactive nature of Zn.

6. Outlook and conclusions

In this contribution, after an overview of common selective leaching strategies for the fabrication of 3D nanoporous materials, the applicability of these materials as heterogeneous (electro)catalysts for the conversion of renewable energy resources into fuels and other valuable chemicals is discussed. The high internal surface area, high density of

active catalytic sites, and remarkable intrinsic properties of these 3D nanoporous materials make them very attractive for large scale applications. (Electro)catalytic processes discussed in this review include, water oxidation, methanol and carbon dioxide reductions. Bulk nanoporous structures made by selective leaching can be used either directly as high-performance (electro)catalysts, or indirectly as 3D bulk current collectors along with poorly conducting (electro)catalyst materials, achieving greatly enhanced catalytic performance in both situations. While traditional 2D thin film water oxidation electrocatalysts perform very well in the thin film format (a few nanometers thickness), the absence of robustness in these films restricts their use in practical devices such as water electrolyzes.

Bulk nanoporous materials seem to be the best solution as they combine the robustness of macroscale materials with the remarkable (electro)catalytic properties of nanoscale structures. In fact, several recent reports have demonstrated the high performance dealloyed bulk nanoporous NiFe-based systems as water oxidation electrocatalysts. Some drawbacks of nanoporous heterogeneous electrocatalysts are highlighted, including the material costs in the case of noble metals, and the long-term stability associated with coarsening during electrocatalytic processes.

Along these lines of developments nanoporous metals can be used both as template and as catalyst. Recently a solid-state-growth approach for the synthesis of 3D interconnected bicontinuous nanoporous graphene with the aid of nanoporous Ni templates was designed [138], but importantly at low temperatures (600–800 °C) representing the actual novelty. It was shown that the pore size can be tuned through the low-temperature solid-state-growth method and in fact the nanoporous Ni template plays a double role, both as nanoporous template and as catalyst for graphene growth. Besides in energy storage, porous graphene is also examined for application in batteries [139]. Interestingly the size of tubular pores could be tailored from tens of nanometers to hundreds of nanometers by adjusting the nanoporous Ni templates and the work provides in our view a competitive strategy for large-scale manufacturing of nanoporous graphene and for design of electrochemical energy storage devices.

Moving forward, the performance of dealloyed 3D nanoporous catalyst materials can further be improved through structural design. Here we believe that the ultimate architecture for this type of applications should involve hierarchical porous structures, where the big porous structures will account for mass transfer in/out the bulk of the material, while the small pore structures provide a large internal surface area for the catalytic reaction. Another way to effectively take advantage of nanoporous architectures in (electro)catalysis is by building upon previous work in the field. Indeed, after several decades of research in the field of catalysis, many high-performance (electro) catalysts have been identified. Therefore, since to date roughly any type nanoporous material can be made owing the various new dealloying strategies, it should be possible to make nanoporous architecture of any material identified as high-performance (electro)catalyst.

Acknowledgements

The authors are thankful to Penn Engineering for the financial support through ED startup.

References

[1] E. Amsterdam, J.H.B. de Vries, J.T.M. De Hosson, P.R. Onck, The influence of strain-induced damage on the mechanical response of open-cell aluminum foam, Acta Mater. 56 (2008) 609–618, http://dx.doi.org/10.1016/j.actamat.2007.10.034.

[2] E. Amsterdam, P.R. Onck, J.T.M. De Hosson, Fracture and microstructure of open cell aluminum foam, J. Mater. Sci. 40 (2005) 5813–5819, http://dx.doi.org/10.1007/s10853-005-4995-8.

[3] J. Baumeister, J. Banhart, M. Weber, Aluminium foams for transport industry, Mater. Des. 18 (1997) 217–220, http://dx.doi.org/10.1016/S0261-3069(97)00050-2.

[4] J.W. Paek, B.H. Kang, S.Y. Kim, J.M. Hyun, Effective thermal conductivity and permeability of aluminum foam materials, Int. J. Thermophys. 21 (2000) 453–464, http://dx.doi.org/10.1023/A:1006643815323.

[5] L.C. Nagle, J.F. Rohan, Nanoporous gold anode catalyst for direct borohydride fuel cell, Int. J. Hydrogen Energy, 2011, pp. 10319–10326, , http://dx.doi.org/10.1016/j.ijhydene.2010.09.077.

[6] X.Y. Lang, H.T. Yuan, Y. Iwasa, M.W. Chen, Three-dimensional nanoporous gold for electrochemical supercapacitors, Scr. Mater. 64 (2011) 923–926, http://dx.doi.org/10.1016/j.scriptamat.2011.01.038.

[7] S.D. Gittard, B.E. Pierson, C.M. Ha, C.-A.M. Wu, R.J. Narayan, D.B. Robinson, Supercapacitive transport of pharmacologic agents using nanoporous gold electrodes, Biotechnol. J. 5 (2010) 192–200, http://dx.doi.org/10.1002/biot.200900250.

[8] M.S. Yavuz, Y. Cheng, J. Chen, C.M. Cobley, Q. Zhang, M. Rycenga, J. Xie, C. Kim, K.H. Song, A.G. Schwartz, L.V. Wang, Y. Xia, Gold nanocages covered by smart polymers for controlled release with near-infrared light, Nat. Mater. 8 (2009) 935–939, http://dx.doi.org/10.1038/nmat2564.

[9] L. Au, D. Zheng, F. Zhou, Z.-Y. Li, X. Li, Y. Xia, A quantitative study on the photothermal effect of immuno gold nanocages targeted to breast cancer cells, ACS Nano 2 (2008) 1645–1652, http://dx.doi.org/10.1021/nn800370j.

[10] C. Cheng, A.H.W. Ngan, Reversible electrochemical actuation of metallic nanohoneycombs induced by pseudocapacitive redox processes, ACS Nano 9 (2015) 3984–3995, http://dx.doi.org/10.1021/nn507466n.

[11] J. Biener, A. Wittstock, T.F. Baumann, J. Weissmüller, M. Bäumer, A.V. Hamza, Surface chemistry in nanoscale materials, Materials (Basel) 2 (2009) 2404–2428, http://dx.doi.org/10.3390/ma2042404.

[12] J. Wang, D.C.C. Lam, Model and analysis of size-stiffening in nanoporous cellular solids, J. Mater. Sci. 44 (2009) 985–991, http://dx.doi.org/10.1007/s10853-008-3219-4.

[13] H.B. Goyal, D. Seal, R.C. Saxena, Bio-fuels from thermochemical conversion of renewable resources: a review, Renew. Sust. Energ. Rev. 12 (2008) 504–517, http://dx.doi.org/10.1016/j.rser.2006.07.014.

[14] J.C. Serrano-Ruiz, R.M. West, J.A. Dumesic, Catalytic conversion of renewable biomass resources to fuels and chemicals, Annu. Rev. Chem. Biomol. Eng. 1 (2010) 79–100, http://dx.doi.org/10.1146/annurev-chembioeng-073009-100935.

[15] J.M. Marchetti, V.U. Miguel, A.F. Errazu, Possible methods for biodiesel production, Renew. Sust. Energ. Rev. 11 (2007) 1300–1311, http://dx.doi.org/10.1016/j.rser.2005.08.006.

[16] A. Birla, B. Singh, S.N. Upadhyay, Y.C. Sharma, Kinetics studies of synthesis of biodiesel from waste frying oil using a heterogeneous catalyst derived from snail shell, Bioresour. Technol. 106 (2012) 95–100, http://dx.doi.org/10.1016/j.biortech.2011.11.065.

[17] Q. Lu, J. Rosen, Y. Zhou, G.S. Hutchings, Y.C. Kimmel, J.G. Chen, F. Jiao, A selective and efficient electrocatalyst for carbon dioxide reduction, Nat. Commun. 5 (2014), http://dx.doi.org/10.1038/ncomms4242.

[18] Y.-C. Hsieh, S.D. Senanayake, Y. Zhang, W. Xu, D.E. Polyansky, Effect of chloride anions on the synthesis and enhanced catalytic activity of silver nanocoral electrodes for CO_2 electroreduction, ACS Catal. 5 (2015) 5349–5356, http://dx.doi.org/10.1021/acscatal.5b01235.

[19] A. Wittstock, V. Zielasek, J. Biener, C.M. Friend, M. Bäumer, Nanoporous gold catalysts for selective gas-phase oxidative coupling of methanol at low temperature, Science 327 (2010) 319–322, http://dx.doi.org/10.1126/science.1183591 (80-.).

[20] J. Zhang, P. Liu, H. Ma, Y. Ding, Nanostructured porous gold for methanol electrooxidation, J. Phys. Chem. C 111 (2007) 10382–10388, http://dx.doi.org/10.1021/jp072333p.

[21] E. Detsi, J.B. Cook, B.K. Lesel, C.L. Turner, Y.-L. Liang, S. Robbennolt, S.H. Tolbert, Mesoporous Ni60Fe30Mn10-alloy based metal/metal oxide composite thick films as highly active and robust oxygen evolution catalysts, Energy Environ. Sci. 9 (2016) 540–549, http://dx.doi.org/10.1039/C5EE02509E.

[22] J.K. Hurst, In pursuit of water oxidation catalysts for solar fuel production, Science 328 (2010) 315–316, http://dx.doi.org/10.1126/science.1187721 (80-.).

[23] Q. Cheng, Y. Wang, J. Jiang, Z. Zou, Y. Zhou, J. Fang, H. Yang, Shape-controlled porous heterogeneous PtRu/C/Nafion microspheres enabling high performance direct methanol fuel cells, J. Mater. Chem. A 3 (2015) 15177–15183, http://dx.doi.org/10.1039/C5TA02627J.

[24] S.J. Davis, K. Caldeira, H.D. Matthews, Future CO_2 emissions and climate change from existing energy infrastructure, Science 329 (2010) 1330–1333, http://dx.doi.org/10.1126/science.1188566.

[25] N.S. Lewis, D.G. Nocera, Powering the planet: chemical challenges in solar energy utilization, Proc. Natl. Acad. Sci. 103 (2006) 15729–15735, http://dx.doi.org/10.1073/pnas.0603395103.

[26] J. Qiao, Y. Liu, F. Hong, J. Zhang, A review of catalysts for the electroreduction of carbon dioxide to produce low-carbon fuels, Chem. Soc. Rev. 43 (2014) 631–675, http://dx.doi.org/10.1039/C3CS60323G.

[27] L. Hammarström, S. Hammes-Schiffer, Guest Editorial, Artificial photosynthesis and solar fuels, Acc. Chem. Res. 42 (2009) 1859–1860, http://dx.doi.org/10.1021/ar900267k.

[28] R. Angamuthu, P. Byers, M. Lutz, A.L. Spek, E. Bouwman, Electrocatalytic CO_2 conversion to oxalate by a copper complex, Science 327 (2010) 313–315, http://dx.doi.org/10.1126/science.1177981 (80-.).

[29] Z. Chen, J.J. Concepcion, M.K. Brennaman, P. Kang, M.R. Norris, P.G. Hoertz, T.J. Meyer, Splitting CO_2 into CO and O_2 by a single catalyst, Proc. Natl. Acad. Sci. 109 (2012) 15606–15611, http://dx.doi.org/10.1073/pnas.1203122109.

[30] Y. Hori, Electrochemical CO_2 reduction on metal electrodes, Mod. Asp. Electrochem, 2008, pp. 89–189, , http://dx.doi.org/10.1007/978-0-387-49489-

0_3.
[31] M.R. Dubois, D.L. Dubois, Development of molecular electrocatalysts for CO_2 reduction and H_2 production/oxidation, Acc. Chem. Res. 42 (2009) 1974–1982, http://dx.doi.org/10.1021/ar900110c.
[32] K. Chandrasekaran, L.O.M. Bockris, In-situ spectroscopic investigation of adsorbed intermediate radicals in electrochemical reactions: CO_2^- on platinum, Surf. Sci. 185 (1987) 495–514, http://dx.doi.org/10.1016/S0039-6028(87)80173-5.
[33] J. Erlebacher, M.J. Aziz, A. Karma, N. Dimitrov, K. Sieradzki, Evolution of nanoporosity in dealloying, Nature 410 (2001) 450–453, http://dx.doi.org/10.1038/35068529.
[34] E. Detsi, Z. Vuković, S. Punzhin, P.M. Bronsveld, P.R. Onck, J.T.M. De Hosson, Fine-tuning the feature size of nanoporous silver, CrystEngComm 14 (2012) 5402–5406, http://dx.doi.org/10.1039/c2ce25313e.
[35] E. Detsi, M. Van De Schootbrugge, S. Punzhin, P.R. Onck, J.T.M. De Hosson, On tuning the morphology of nanoporous gold, Scr. Mater. 64 (2011), http://dx.doi.org/10.1016/j.scriptamat.2010.10.023.
[36] T.L. Maxwell, T.J. Balk, The fabrication and characterization of bimodal nanoporous Si with retained mg through dealloying, Adv. Eng. Mater. 1700519 (2017) 1–9, http://dx.doi.org/10.1002/adem.201700519.
[37] E. Seker, M.L. Reed, M.R. Begley, Nanoporous gold: fabrication, characterization, and applications, Materials (Basel) 2 (2009) 2188–2215, http://dx.doi.org/10.3390/ma2042188.
[38] J.R. Hayes, A.M. Hodge, J. Biener, A.V. Hamza, K. Sieradzki, Monolithic nanoporous copper by dealloying Mn–Cu, J. Mater. Res. 21 (2006) 2611–2616, http://dx.doi.org/10.1557/jmr.2006.0322.
[39] J. Biener, A. Wittstock, L.A. Zepeda-Ruiz, M.M. Biener, V. Zielasek, D. Kramer, R.N. Viswanath, J. Weissmüller, M. Bäumer, A.V. Hamza, Surface-chemistry-driven actuation in nanoporous gold, Nat. Mater. 8 (2009) 47–51, http://dx.doi.org/10.1038/nmat2335.
[40] X. Lang, L. Zhang, T. Fujita, Y. Ding, M. Chen, Three-dimensional bicontinuous nanoporous Au/polyaniline hybrid films for high-performance electrochemical supercapacitors, J. Power Sources 197 (2012) 325–329, http://dx.doi.org/10.1016/j.jpowsour.2011.09.006.
[41] J. Snyder, I. McCue, K. Livi, J. Erlebacher, Structure/processing/properties relationships in nanoporous nanoparticles as applied to catalysis of the cathodic oxygen reduction reaction, J. Am. Chem. Soc. 134 (2012) 8633–8645, http://dx.doi.org/10.1021/ja3019498.
[42] a.M. Hodge, J. Biener, J.R. Hayes, P.M. Bythrow, C.a. Volkert, a.V. Hamza, Scaling equation for yield strength of nanoporous open-cell foams, Acta Mater. 55 (2007) 1343–1349, http://dx.doi.org/10.1016/j.actamat.2006.09.038.
[43] Y.C.K. Chen, Y.S. Chu, J. Yi, I. McNulty, Q. Shen, P.W. Voorhees, D.C. Dunand, Morphological and topological analysis of coarsened nanoporous gold by X-ray nanotomography, Appl. Phys. Lett. 96 (2010), http://dx.doi.org/10.1063/1.3285175.
[44] Q. Chen, K. Sieradzki, Spontaneous evolution of bicontinuous nanostructures in dealloyed Li-based systems, Nat. Mater. 12 (2013) 1102–1106, http://dx.doi.org/10.1038/nmat3741.
[45] H. Yaghoobnejad Asl, J. Fu, H. Kumar, S.S. Welborn, V.B. Shenoy, E. Detsi, In situ dealloying of bulk Mg2Sn in Mg-Ion half cell as an effective route to nanostructured Sn for high performance Mg-ion battery anodes, Chem. Mater. (2018), http://dx.doi.org/10.1021/acs.chemmater.7b04124.
[46] T. Wada, K. Yubuta, A. Inoue, H. Kato, Dealloying by metallic melt, Mater. Lett. 65 (2011) 1076–1078, http://dx.doi.org/10.1016/j.matlet.2011.01.054.
[47] Z. Lu, C. Li, J. Han, F. Zhang, P. Liu, H. Wang, Z. Wang, C. Cheng, L. Chen, A. Hirata, T. Fujita, J. Erlebacher, M. Chen, Three-dimensional bicontinuous nanoporous materials by vapor phase dealloying, Nat. Commun. 9 (2018) 276, http://dx.doi.org/10.1038/s41467-017-02167-y.
[48] M.G. Walter, E.L. Warren, J.R. McKone, S.W. Boettcher, Q. Mi, E. a Santori, N.S. Lewis, Solar water splitting cells, Chem. Rev. 110 (2010) 6446–6473, http://dx.doi.org/10.1021/Cr1002326.
[49] C.C.L. McCrory, S. Jung, J.C. Peters, T.F. Jaramillo, Benchmarking heterogeneous electrocatalysts for the oxygen evolution reaction, J. Am. Chem. Soc. 135 (45) (2013) 16977–16987 http://pubs.acs.org/doi/abs/10.1021/ja407115p.
[50] M.W. Kanan, D.G. Nocera, In situ formation of an oxygen-evolving catalyst in neutral water containing phosphate and Co^{2+}, Science 321 (2008) 1072–1075, http://dx.doi.org/10.1126/science.1162018 (80-.).
[51] M. Gong, H. Dai, A mini review of NiFe-based materials as highly active oxygen evolution reaction electrocatalysts, Nano Res. 8 (2014) 23–39, http://dx.doi.org/10.1007/s12274-014-0591-z.
[52] A.J. Esswein, Y. Surendranath, S.Y. Reece, D.G. Nocera, Highly active cobalt phosphate and borate based oxygen evolving catalysts operating in neutral and natural waters, Energy Environ. Sci. 4 (2011) 499, http://dx.doi.org/10.1039/c0ee00518e.
[53] M.G. Walter, E.L. Warren, J.R. McKone, S.W. Boettcher, Q. Mi, E.A. Santori, N.S. Lewis, Solar water splitting cells, Chem. Rev. 110 (2010) 6446–6473, http://dx.doi.org/10.1021/cr1002326.
[54] K. Michelsen, H. De Raedt, J.T.M. De Hosson, Aspects of mathematical morphology, Adv. Imaging Electron Phys. 125 (2003) 119–194, http://dx.doi.org/10.1016/S1076-5670(02)80016-7.
[55] J. Luo, J. Im, M.T. Mayer, M. Schreier, M.K. Nazeeruddin, N. Park, S.D. Tilley, H.J. Fan, M. Grätzel, Water photolysis at 12.3% efficiency via perovskite photovoltaics and Earth-abundant catalysts, Science 345 (2014) 1593–1596 (80-.).
[56] X. Lu, C. Zhao, Electrodeposition of hierarchically structured densities, Nat. Commun. 6 (2015) 1–7, http://dx.doi.org/10.1038/ncomms7616.
[57] W. Zhou, X.-J. Wu, X. Cao, X. Huang, C. Tan, J. Tian, H. Liu, J. Wang, H. Zhang, Ni_3S_2 nanorods/Ni foam composite electrode with low overpotential for electrocatalytic oxygen evolution, Energy Environ. Sci. 6 (2013) 2921, http://dx.doi.org/10.1039/c3ee41572d.
[58] J. Wang, H. Zhong, Y. Qin, X. Zhang, An efficient three-dimensional oxygen evolution electrode, Angew. Chem. 125 (2013) 5356–5361, http://dx.doi.org/10.1002/ange.201301066.
[59] Y. Qiu, L. Xin, W. Li, Electrocatalytic oxygen evolution over supported small amorphous ni-fe nanoparticles in alkaline electrolyte, Langmuir 30 (2014) 7893–7901, http://dx.doi.org/10.1021/la501246e.
[60] X. Yu, M. Zhang, W. Yuan, G. Shi, A high-performance three-dimensional Ni-Fe layered double hydroxide/graphene electrode for water oxidation, J. Mater. Chem. 3 (2015) 6921–6928.
[61] M.W. Louie, A.T. Bell, An investigation of thin-film Ni-Fe oxide catalysts for the electrochemical evolution of oxygen, J. Am. Chem. Soc. 135 (2013) 12329–12337, http://dx.doi.org/10.1021/ja405351s.
[62] M. Gong, H. Dai, A mini review of NiFe-based materials as highly active oxygen evolution reaction electrocatalysts, Nano Res. 8 (2014) 23–39, http://dx.doi.org/10.1007/s12274-014-0591-z.
[63] Z. Tang, C. Tang, H. Gong, A high energy density asymmetric supercapacitor from nano-architectured Ni(OH)2/carbon nanotube electrodes, Adv. Funct. Mater. 22 (2012) 1272–1278, http://dx.doi.org/10.1002/adfm.201102796.
[64] S. Zhu, X. Yang, W. Yang, L. Zhang, J. Wang, M. Huo, Application of porous nickel-coated TiO_2 for the photocatalytic degradation of aqueous quinoline in an internal airlift loop reactor, Int. J. Environ. Res. Public Health 9 (2012) 548–563, http://dx.doi.org/10.3390/ijerph9020548.
[65] N.A. Jarrah, J.G. Van Ommen, L. Lefferts, (CNFs); a new structured catalyst support, Prepr. Pap. - Am. Chem. Soc., Div. Fuel Chem. 49 (2004) 881–882.
[66] E. Detsi, E. De Jong, A. Zinchenko, Z. Vuković, I. Vuković, S. Punzhin, K. Loos, G. Ten Brinke, H.A. De Raedt, P.R. Onck, J.T.M. De Hosson, On the specific surface area of nanoporous materials, Acta Mater. 59 (2011), http://dx.doi.org/10.1016/j.actamat.2011.08.025.
[67] Y.H. Tan, J.a. Davis, K. Fujikawa, N.V. Ganesh, A.V. Demchenko, K.J. Stine, Surface area and pore size characteristics of nanoporous gold subjected to thermal, mechanical, or surface modification studied using gas adsorption isotherms, cyclic voltammetry, thermogravimetric analysis, and scanning electron microscopy, J. Mater. Chem. 22 (2012) 6733, http://dx.doi.org/10.1039/c2jm16633j.
[68] C. Dong, T. Kou, H. Gao, Z. Peng, Z. Zhang, Eutectic-derived mesoporous Ni-Fe-O nanowire network catalyzing oxygen evolution and overall water splitting, Adv. Energy Mater. 1701347 (2017) 1–9, http://dx.doi.org/10.1002/AENM.201701347.
[69] P. Zhang, L. Li, D. Nordlund, H. Chen, L. Fan, B. Zhang, X. Sheng, Q. Daniel, L. Sun, Dendritic core-shell nickel-iron-copper metal/metal oxide electrode for efficient electrocatalytic water oxidation, Nat. Commun. 9 (2018) 381, http://dx.doi.org/10.1038/s41467-017-02429-9.
[70] G. He, Z. Li, J. Zhao, S. Wang, H. Wu, M.D. Guiver, Z. Jiang, Nanostructured ion-exchange membranes for fuel cells: recent advances and perspectives, Adv. Mater. 27 (2015) 5280–5295, http://dx.doi.org/10.1002/adma.201501406.
[71] H. Hewa Dewage, B. Wu, A. Tsoi, V. Yufit, G. Offer, N. Brandon, A novel regenerative hydrogen cerium fuel cell for energy storage applications, J. Mater. Chem. A 3 (2015) 9446–9450, http://dx.doi.org/10.1039/C5TA00571J.
[72] Y.E. Seidel, A. Schneider, Z. Jusys, B. Wickman, B. Kasemo, R.J. Behm, Transport effects in the electrooxidation of methanol studied on nanostructured Pt/glassy carbon electrodes, Langmuir 26 (2010) 3569–3578, http://dx.doi.org/10.1021/la902962g.
[73] H. Wang, C. Wingender, H. Baltruschat, M. Lopez, M.T. Reetz, Methanol oxidation on Pt, PtRu, and colloidal Pt electrocatalysts: a DEMS study of product formation, J. Electroanal. Chem. 509 (2001) 163–169, http://dx.doi.org/10.1016/S0022-0728(01)00531-9.
[74] H. Wang, L. Zhu, L. Yang, F. Liao, M. Sheng, B. Jiang, M. Shao, Prominent electrocatalytic methanol oxidation from cauli-flower shape gold with high-index facets, Mater. Chem. Phys. 186 (2017) 301–304, http://dx.doi.org/10.1016/j.matchemphys.2016.10.057.
[75] N. Kakati, J. Maiti, S.H. Lee, S.H. Jee, B. Viswanathan, Y.S. Yoon, Anode catalysts for direct methanol fuel cells in acidic media: do we have any alternative for Pt or Pt-Ru? Chem. Rev. 114 (2014) 12397–12429, http://dx.doi.org/10.1021/cr400389f.
[76] Z. Borkowska, A. Tymosiak-Zielinska, G. Shul, Electrooxidation of methanol on polycrystalline and single crystal gold electrodes, Electrochim. Acta, 2004, pp. 1209–1220, , http://dx.doi.org/10.1016/j.electacta.2003.09.046.
[77] G. Tremiliosi-Filho, E.R. Gonzalez, A.J. Motheo, E.M. Belgsir, J.M. Léger, C. Lamy, Electro-oxidation of ethanol on gold: analysis of the reaction products and mechanism, J. Electroanal. Chem. 444 (1998) 31–39, http://dx.doi.org/10.1016/S0022-0728(97)00536-6.
[78] K.A. Assiongbon, D. Roy, Electro-oxidation of methanol on gold in alkaline media: adsorption characteristics of reaction intermediates studied using time resolved electro-chemical impedance and surface plasmon resonance techniques, Surf. Sci. 594 (2005) 99–119, http://dx.doi.org/10.1016/j.susc.2005.07.015.
[79] M. Avramov-Ivić, V. Jovanović, G. Vlajnić, J. Popić, The electrocatalytic properties of the oxides of noble metals in the electro-oxidation of some organic molecules, J. Electroanal. Chem. 423 (1997) 119–124, http://dx.doi.org/10.1016/S0022-0728(96)04787-0.
[80] Z. Borkowska, A. Tymosiak-Zielinska, R. Nowakowski, High catalytic activity of chemically activated gold electrodes towards electro-oxidation of methanol, Electrochim. Acta 49 (2004) 2613–2621, http://dx.doi.org/10.1016/j.electacta.2004.01.030.
[81] M. Graf, M. Haensch, J. Carstens, G. Wittstock, J. Weissmüller, Electrocatalytic methanol oxidation with nanoporous gold: microstructure and selectivity, Nano 9

(2017) 17839–17848, http://dx.doi.org/10.1039/C7NR05124G.
[82] S. Pedireddy, H.K. Lee, C.S.L. Koh, J.M.R. Tan, W.W. Tjiu, X.Y. Ling, Nanoporous gold bowls: a kinetic approach to control open shell structures and size-tunable lattice strain for electrocatalytic applications, Small (2016) 4531–4540, http://dx.doi.org/10.1002/smll.201601371.
[83] Y. Xu, X. Ke, C. Yu, S. Liu, J. Zhao, G. Cui, D. Higgins, Z. Chen, Q. Li, G. Wu, A strategy for fabricating nanoporous gold films through chemical dealloying of electrochemically deposited Au-Sn alloys, Nanotechnology 25 (2014), http://dx.doi.org/10.1088/0957-4484/25/44/445602.
[84] M. Graf, B. Roschning, Nanoporous Gold by Alloy Corrosion: Method-structure-property, vol. 164, (2017), pp. 194–200, http://dx.doi.org/10.1149/2.1681704jes.
[85] S. Cattarin, D. Kramer, A. Lui, M.M. Musiani, Preparation and characterization of gold nanostructures of controlled dimension by electrochemical techniques, J. Phys. Chem. C 111 (2007) 12643–12649, http://dx.doi.org/10.1021/jp072405c.
[86] T. Krekeler, A.V. Straßer, M. Graf, K. Wang, C. Hartig, M. Ritter, J. Weissmüller, Silver-rich clusters in nanoporous gold, Mater. Res. Lett. 5 (2017) 314–321, http://dx.doi.org/10.1080/21663831.2016.1276485.
[87] J. Weissmüller, R.C. Newman, H.-J. Jin, A.M. Hodge, J.W. Kysar, Nanoporous metals by alloy corrosion: formation and mechanical properties, MRS Bull. 34 (2009) 577–586, http://dx.doi.org/10.1557/mrs2009.157.
[88] A.P. O'Mullane, From single crystal surfaces to single atoms: investigating active sites in electrocatalysis, Nano 6 (2014) 4012–4026, http://dx.doi.org/10.1039/C4NR00419A.
[89] H. Okamoto, T. Gojuki, N. Okano, T. Kuge, M. Morita, A. Maruyama, Y. Mukouyama, Oxidation of formic acid and methanol and their potential oscillations under no or little water conditions, Electrochim. Acta 136 (2014) 385–395, http://dx.doi.org/10.1016/j.electacta.2014.05.135.
[90] X. Liu, R.J. Madix, C.M. Friend, Unraveling molecular transformations on surfaces: a critical comparison of oxidation reactions on coinage metals, Chem. Soc. Rev. 37 (2008) 2243, http://dx.doi.org/10.1039/b800309m.
[91] M. Zlokarnik, Ullmann's encyclopedia of industrial chemistry, Ullmann's Encycl. Ind. Chem. 25 (2012) 1-25.40, , http://dx.doi.org/10.1002/14356007.b02.
[92] X. Ge, R. Wang, P. Liu, Y. Ding, Platinum-decorated nanoporous gold leaf for methanol electrooxidation, Chem. Mater. 19 (2007) 5827–5829, http://dx.doi.org/10.1021/cm702335f.
[93] X. Wang, W. Wang, Z. Qi, C. Zhao, H. Ji, Z. Zhang, Electrochemical catalytic activities of nanoporous palladium rods for methanol electro-oxidation, J. Power Sources 195 (2010) 6740–6747, http://dx.doi.org/10.1016/j.jpowsour.2010.03.098.
[94] Z.P. Sun, X.G. Zhang, Y.Y. Liang, H.L. Li, A facile approach towards sulfonate functionalization of multi-walled carbon nanotubes as Pd catalyst support for ethylene glycol electro-oxidation, J. Power Sources 191 (2009) 366–370, http://dx.doi.org/10.1016/j.jpowsour.2009.01.093.
[95] C. Xu, Y. Liu, D. Yuan, Pt and Pd supported on carbon microspheres for alcohol electrooxidation in Alkaline media, Int. J. Electrochem. Sci. 2 (2007) 674–680.
[96] Y.W. Lee, S.B. Han, K.W. Park, Electrochemical properties of Pd nanostructures in alkaline solution, Electrochem. Commun. 11 (2009) 1968–1971, http://dx.doi.org/10.1016/j.elecom.2009.08.030.
[97] Z.X. Liang, T.S. Zhao, J.B. Xu, L.D. Zhu, Mechanism study of the ethanol oxidation reaction on palladium in alkaline media, Electrochim. Acta 54 (2009) 2203–2208, http://dx.doi.org/10.1016/j.electacta.2008.10.034.
[98] X. Wang, W. Wang, Z. Qi, C. Zhao, H. Ji, Z. Zhang, High catalytic activity of ultrafine nanoporous palladium for electro-oxidation of methanol, ethanol, and formic acid, Electrochem. Commun. 11 (2009) 1896–1899, http://dx.doi.org/10.1016/j.elecom.2009.08.011.
[99] H. Razmi, E. Habibi, H. Heidari, Electrocatalytic oxidation of methanol and ethanol at carbon ceramic electrode modified with platinum nanoparticles, Electrochim. Acta 53 (2008) 8178–8185, http://dx.doi.org/10.1016/j.electacta.2008.06.033.
[100] W. Zhou, C. Zhai, Y. Du, J. Xu, P. Yang, Electrochemical fabrication of novel platinum-poly(5-nitroindole) composite catalyst and its application for methanol oxidation in alkaline medium, Int. J. Hydrog. Energy 34 (2009) 9316–9323, http://dx.doi.org/10.1016/j.ijhydene.2009.09.059.
[101] D.J. Guo, H.L. Li, Highly dispersed Ag nanoparticles on functional MWNT surfaces for methanol oxidation in alkaline solution, Carbon 43 (2005) 1259–1264, http://dx.doi.org/10.1016/j.carbon.2004.12.021.
[102] J. Zeng, J. Yang, J.Y. Lee, W. Zhou, Preparation of carbon-supported core-shell Au-Pt nanoparticles for methanol oxidation reaction: the promotional effect of the Au core, J. Phys. Chem. B 110 (2006) 24606–24611, http://dx.doi.org/10.1021/jp0640979.
[103] L. Dong, R.R.S. Gari, Z. Li, M.M. Craig, S. Hou, Graphene-supported platinum and platinum-ruthenium nanoparticles with high electrocatalytic activity for methanol and ethanol oxidation, Carbon 48 (2010) 781–787, http://dx.doi.org/10.1016/j.carbon.2009.10.027.
[104] A.S. Aricò, P. Bruce, B. Scrosati, J.-M. Tarascon, W. van Schalkwijk, Nanostructured materials for advanced energy conversion and storage devices, Nat. Mater. 4 (2005) 366–377, http://dx.doi.org/10.1038/nmat1368.
[105] L.H. Yu, C.H. Kuo, C.T. Yeh, Poly(vinylpyrrolidone)-modified graphite carbon nanofibers as promising supports for PtRu catalysts in direct methanol fuel cells, J. Am. Chem. Soc. 129 (2007) 9999–10010, http://dx.doi.org/10.1021/ja072367a.
[106] B.A. Rosen, A. Salehi-Khojin, M.R. Thorson, W. Zhu, D.T. Whipple, P.J.A. Kenis, R.I. Masel, Ionic liquid-mediated selective conversion of CO_2 to CO at low overpotentials, Science 334 (2011) 643–644, http://dx.doi.org/10.1126/science.1209786 (80-.).
[107] S. Sen, D. Liu, G.T.R. Palmore, Electrochemical reduction of CO_2 at copper nanofoams, ACS Catal. (2014) 3091–3095, http://dx.doi.org/10.1021/cs500522g.
[108] S. Zhang, P. Kang, T.J. Meyer, Nanostructured tin catalysts for selective electrochemical reduction of carbon dioxide to formate, J. Am. Chem. Soc. 136 (2014) 1734–1737, http://dx.doi.org/10.1021/ja4113885.
[109] C.E. Tornow, M.R. Thorson, S. Ma, A.A. Gewirth, P.J.A. Kenis, Nitrogen-based catalysts for the electrochemical reduction of CO_2 to CO, J. Am. Chem. Soc. 134 (2012) 19520–19523, http://dx.doi.org/10.1021/ja308217w.
[110] D. Kim, J. Resasco, Y. Yu, A.M. Asiri, P. Yang, Synergistic geometric and electronic effects for electrochemical reduction of carbon dioxide using gold-copper bimetallic nanoparticles, Nat. Commun. 5 (2014), http://dx.doi.org/10.1038/ncomms5948.
[111] C.W. Li, M.W. Kanan, CO_2 reduction at low overpotential on Cu electrodes resulting from the reduction of thick Cu_2O films, J. Am. Chem. Soc. 134 (2012) 7231–7234, http://dx.doi.org/10.1021/ja3010978.
[112] K. Manthiram, B.J. Beberwyck, A.P. Alivisatos, Enhanced electrochemical methanation of carbon dioxide with a dispersible nanoscale copper catalyst, J. Am. Chem. Soc. 136 (2014) 13319–13325, http://dx.doi.org/10.1021/ja5065284.
[113] J.A. Dean, Lange's handbook of chemistry, Mater. Manuf. Process. 5 (1990) 687–688, http://dx.doi.org/10.1080/10426919008953291.
[114] H.A. Schwarz, R.W. Dodson, Reduction potentials of CO_2^- and the alcohol radicals, J. Phys. Chem. 93 (1989) 409–414, http://dx.doi.org/10.1021/j100338a079.
[115] Y. Hori, A. Murata, K. Kikuchi, S. Suzuki, Electrochemical reduction of carbon dioxide to carbon monoxide at a gold electrode in aqueous potassium hydrogen carbonate, J. Chem. Soc. Chem. Commun. (1987) 728–729, http://dx.doi.org/10.1039/c39870000728.
[116] J. Rosen, G.S. Hutchings, Q. Lu, S. Rivera, Y. Zhou, D.G. Vlachos, F. Jiao, Mechanistic insights into the electrochemical reduction of CO_2 to CO on nanostructured Ag surfaces, ACS Catal. 5 (2015) 4293–4299, http://dx.doi.org/10.1021/acscatal.5b00840.
[117] M. Gattrell, N. Gupta, A. Co, A review of the aqueous electrochemical reduction of CO_2 to hydrocarbons at copper, J. Electroanal. Chem. 594 (2006) 1–19, http://dx.doi.org/10.1016/j.jelechem.2006.05.013.
[118] N. Hoshi, M. Kato, Y. Hori, Electrochemical reduction of CO_2 on single crystal electrodes of silver, J. Electroanal. Chem. 440 (1997) 283–286, http://dx.doi.org/10.1016/S0022-0728(97)00447-6.
[119] E.E. Benson, M.D. Sampson, K.A. Grice, J.M. Smieja, J.D. Froehlich, D. Friebel, J.A. Keith, E.A. Carter, A. Nilsson, C.P. Kubiak, The electronic states of rhenium bipyridyl electrocatalysts for CO_2 reduction as revealed by X-ray absorption spectroscopy and computational quantum chemistry, Angew. Chem. Int. Ed. 52 (2013) 4841–4844, http://dx.doi.org/10.1002/anie.201209911.
[120] P. Kang, C. Cheng, Z. Chen, C.K. Schauer, T.J. Meyer, M. Brookhart, Selective electrocatalytic reduction of CO_2 to formate by water-stable iridium dihydride pincer complexes, J. Am. Chem. Soc. 134 (2012) 5500–5503, http://dx.doi.org/10.1021/ja300543s.
[121] A. Salehi-Khojin, H.R.M. Jhong, B.A. Rosen, W. Zhu, S. Ma, P.J.A. Kenis, R.I. Masel, Nanoparticle silver catalysts that show enhanced activity for carbon dioxide electrolysis, J. Phys. Chem. C 117 (2013) 1627–1632, http://dx.doi.org/10.1021/jp310509z.
[122] Z. Deng, E. Detsi, Enhancing the free corrosion dealloying rate with a catalytically driven reaction, Nano 9 (2017), http://dx.doi.org/10.1039/c7nr04611a.
[123] Y. Yoon, A.S. Hall, Y. Surendranath, Tuning of silver catalyst mesostructure promotes selective carbon dioxide conversion into fuels, Angew. Chem. Int. Ed. 55 (2016) 15282–15286, http://dx.doi.org/10.1002/anie.201607942.
[124] Y. Chen, C.W. Li, M.W. Kanan, Aqueous CO_2 reduction at very low overpotential on oxide-derived au nanoparticles, J. Am. Chem. Soc. 134 (2012) 19969–19972, http://dx.doi.org/10.1021/ja309317u.
[125] T. Hatsukade, K.P. Kuhl, E.R. Cave, D.N. Abram, T.F. Jaramillo, Insights into the electrocatalytic reduction of CO_2 on metallic silver surfaces, Phys. Chem. Chem. Phys. 16 (2014) 13814–13819, http://dx.doi.org/10.1039/C4CP00692E.
[126] Y. Chen, M.W. Kanan, Tin oxide dependence of the CO_2 reduction efficiency on tin electrodes and enhanced activity for tin/tin oxide thin-film catalysts, J. Am. Chem. Soc. 134 (2012) 1986–1989, http://dx.doi.org/10.1021/ja2108799.
[127] J. Kibsgaard, Z. Chen, B.N. Reinecke, T.F. Jaramillo, Engineering the surface structure of MoS_2 to preferentially expose active edge sites for electrocatalysis, Nat. Mater. 11 (2012) 963–969, http://dx.doi.org/10.1038/nmat3439.
[128] Z. Chen, D. Cummins, B.N. Reinecke, E. Clark, M.K. Sunkara, T.F. Jaramillo, Core-shell MoO_3-MoS_2 nanowires for hydrogen evolution: a functional design for electrocatalytic materials, Nano Lett. 11 (2011) 4168–4175, http://dx.doi.org/10.1021/nl2020476.
[129] H. Mistry, R. Reske, Z. Zeng, Z.J. Zhao, J. Greeley, P. Strasser, B.R. Cuenya, Exceptional size-dependent activity enhancement in the electroreduction of CO_2 over Au nanoparticles, J. Am. Chem. Soc. 136 (2014) 16473–16476, http://dx.doi.org/10.1021/ja508879j.
[130] A.S. Hall, Y. Yoon, A. Wuttig, Y. Surendranath, Mesostructure-induced selectivity in CO_2 reduction catalysis, J. Am. Chem. Soc. 137 (2015) 14834–14837, http://dx.doi.org/10.1021/jacs.5b08259.
[131] P. Rodríguez, A.A. Koverga, M.T.M. Koper, Carbon monoxide as a promoter for its own oxidation on a gold electrode, Angew. Chem. Int. Ed. 49 (2010) 1241–1243, http://dx.doi.org/10.1002/anie.200905387.
[132] P. Rodriguez, J.M. Feliu, M.T.M. Koper, Unusual adsorption state of carbon monoxide on single-crystalline gold electrodes in alkaline media, Electrochem. Commun. 11 (2009) 1105–1108, http://dx.doi.org/10.1016/j.elecom.2009.03.018.
[133] P. Rodriguez, Y. Kwon, M.T.M. Koper, The promoting effect of adsorbed carbon monoxide on the oxidation of alcohols on a gold catalyst, Nat. Chem. 4 (2012) 177–182, http://dx.doi.org/10.1038/nchem.1221.

[134] J. Rosen, G.S. Hutchings, Q. Lu, R.V. Forest, A. Moore, F. Jiao, Electrodeposited Zn dendrites with enhanced CO selectivity for electrocatalytic CO_2 reduction, ACS Catal. 5 (2015) 4586–4591, http://dx.doi.org/10.1021/acscatal.5b00922.
[135] K.P. Kuhl, T. Hatsukade, E.R. Cave, D.N. Abram, J. Kibsgaard, T.F. Jaramillo, Electrocatalytic conversion of carbon dioxide to methane and methanol on transition metal surfaces, J. Am. Chem. Soc. 136 (2014) 14107–14113, http://dx.doi.org/10.1021/ja505791r.
[136] F. Quan, D. Zhong, H. Song, F. Jia, L. Zhang, A highly efficient zinc catalyst for selective electroreduction of carbon dioxide in aqueous NaCl solution, J. Mater. Chem. A 3 (2015) 16409–16413, http://dx.doi.org/10.1039/C5TA04102C.
[137] X. Jiang, F. Cai, D. Gao, J. Dong, S. Miao, G. Wang, X. Bao, Electrocatalytic reduction of carbon dioxide over reduced nanoporous zinc oxide, Electrochem. Commun. 68 (2016) 67–70, http://dx.doi.org/10.1016/j.elecom.2016.05.003.
[138] Lu Liqiang, Paul Andela, Jeff Th.M. De Hosson, Yutao Pei, Template-free synthesis of nanoporous nickel and alloys as binder-free current collectors of Li ion batteries, ACS Appl. Nano Mater. (2018 April 19), http://dx.doi.org/10.1021/acsanm.8b00284.
[139] J.S. Luo, J.L. Liu, Z.Y. Zeng, C.F. Ng, L.J. Ma, H. Zhang, J.Y. Lin, Z.X. Shen, H.J. Fan, Three-dimensional graphene foam supported Fe_3O_4 lithium battery anodes with long cycle life and high rate capability, Nano Lett. 13 (2013) 6136–6143.